First Principle Insights into Monofunctional Catalytic
Deoxygenation and C-C and C-O Bond Formation over Cu

_____

A Thesis

Presented to

the faculty of the School of Engineering and Applied Science

University of Virginia

_____

in partial fulfillment

of the requirements for the degree

Master of Science

by

ZHIYUAN TAO

December

2012

APPROVAL SHEET

The thesis

is submitted in partial fulfillment of the requirements

for the degree of

Master of Science

_____
AUTHOR

The thesis has been read and approved by the examining committee:

_____
Advisor

_____

_____

_____

_____

_____

Accepted for the School of Engineering and Applied Science:

_____

Dean, School of Engineering and Applied Science

December

2012

First Principle Insights into Monofunctional Catalytic

Deoxygenation and C-C and C-O Bond Formation over Cu

A Thesis Present to

The Faculty of the School of Engineering and Applied Science

University of Virginia

In Partial Fulfillment

of the Requirement for the Degree

Master of Science

Zhiyuan Tao

Department of Chemical Engineering

Aug. 2012

Abstract

The catalytic pathways involved in C-C (aldol condensation) and C-O (esterification) bond formation reactions of propanal and propanol over Cu are examined in this work by carrying out first-principle density functional theory (DFT) calculations. The reactions of propanal and propanol with minimal hydrogen addition over supported Cu are readily equilibrated via rapid C-H and O-H bond activation to form an equilibrium mixtures. These reactions proceed through the formation of a surface propoxide intermediate ($CH_3CH_2CH_2O*$) that is formed either via the dehydrogenation of propanol or the hydrogenation of propanal, with activation energies of 120 and 56 kJ/mol, respectively. There is direct charge transfer from Cu surface atoms to the adsorbed propoxide intermediate which results in the formation a surface $CH_3CH_2CH_2O(-)$ intermediate that acts as base which catalyzes condensation as well as esterification reactions. This basic propoxide intermediate can readily abstract the acidic hydrogen atom that resides α to the carbonyl of the propanal (aldehyde) to produce an enolate intermediate with an activation barrier of 54 kJ/mol which initiates aldol condensation. The subsequent C-C coupling between the adsorbed enolate and a second propanal proceeds with an activation barrier of only 9 kJ/mol. The basic propoxide intermediate can also directly react with a surface propanal to form a C-O bond and the propyl propionate intermediate with an activation energy of 57 kJ/mol. The theoretical results indicate that the adsorbed propoxide intermediate reacts with the adsorbed aldehyde in the kinetical relevant step in both the condensation and esterification reactions via α-H abstraction of aldehyde and nucleophilic attack on the carbonyl of the aldehyde, respectively. The comparison with the experimental results indicates that apparent activation energy difference between condensation and esterification reaction is within 7-8 kJ/mol with theory suggesting that esterification is slightly more favored whereas the experiments show a very small preference for the aldol condensation reaction.

Table of Contents

Chapter1 Introduction

The increasing demand for scarce and limited petroleum resources has significantly increased the urgency to develop new routes for the production of fuels and chemicals from biomass as well as other sustainable resources [1-3]. The high content of oxygen in biomass, however, prevents its conversion or the converion of its constituent C_5 and C_6 sugars into chemicals or fuels. Catalytic deoxygenation routes are therefore critcal to the development of viable biomass conversion processes. Deoxygenation can typically proceed via hydrogenolysis, dehydration (elimination of H_2O) [1,4] and decarboxylation/decarbonylation (elimination of CO_2, CO) [5,6]. These routes can nominally be divided into paths that require the addition of external hydrogen [7,8] such as hydrogenolysis verses paths that can eliminate oxygen directly. Dumesic *et al.* reported the in-situ process of H_2 generation, such as water-gas shift reaction [2,9], as an internal hydrogen resource replacing external hydrogen, but the low ratio of H/C in biomass molecules makes H_2 an expensive reactant for oxygen removal via dehydration. Alternatively, catalytic decarboxylation/decarbonylation routes have proven to be effective in removing oxygen from biomass molecules [10-12]. These routes eliminate the need for the costly addition of external H_2 or other carbon resources thus making them attractive for the deoxygenation of biomass.

The conversion of biomass into fuels presents the additional challenges of controlling the carbon chain length and degree of branching of resulting hydrocarbon products. The gasification of biomass to syngas (mixture of CO and H_2) [1] followed by Fisher-Tropsch synthesis [13,14] results in broad distribution of products that range from C_1 to C_{50} hydrocarbons [15]. Alternatively, biomass can be converted to C_5 and C_6 sugars via hydrolysis pathways [1], deoxygenated and subsequently converted to linear long-chain hydrocarbons via carbon chain growth processes. As such, there has been a significant increase in research in developing catalysts that can effectively promote C-C bond formation and the formation of controlled chain length and molecular weight distributions [16,17].

Aldol condensation, which provides an effective route to form C-C bonds is used industrially in the synthesis of a range of important chemical intermediates including 2-ethyl hexanol, methyl isobutyl ketone (MIBK) as well as Guerbet alcohols [18]. Aldol condensation typically proceeds by either acid or base catalyzed coupling of aldehydes or alcohols to form β-hydroxy aldehydes/ketones which subsequently dehydrate to form α,β-unsaturated carbonyl intermediates [19]. Base-catalyzed aldol condensation mechanisms are thought to proceed via the abstraction of the acid proton at carbon which is α to the carbonyl thus resulting in formation of an enolate intermediate that can subsequently attack the carbonyl of a second aldehyde molecule to form an intermolecular C-C bond. These reactions can be carried out over a range of different homogeneous catalysts including organometallic Cu(II), Co(II),

Mn(II), and Zn(II) [20] together with base promotors (NaOH, NaOR, and Na_2CO_3) or basic ligands [21-24] or over heterogeneous base catalysts including MgO[25-28], Mg-AlOx, ZnO[29,30], phosphates [31], and promoted meso-porous silicas such as MCM41 [32] and hydrotalcites [33,34]. Theoretical studies of aldol condensation have been carried out over different homogeneous catalysts [20] that show that homogeneous Co(II), Mn(II) and Zn(II) actively catalyze C-C formation with activation barrier between 12-16 kJ/mol, while reactions over Cu(II) is less likely as the barrier is 60 kJ/mol. There are no reported theoretical studies for aldol condensation over heterogeneous catalytic systems that we are aware of.

Similar heterogeneous base-catalyzed reactions have recently been demonstrated for the conversion of oxygenates derived from biomass into longer hydrocarbon intermediates. Dumesic [2,16] demonstrated this via the conversion of sugar molecules to longer chain C_6-C_{12} alkane products via coupling base-catalyzed aldol condensation and dehydration routes [2,16].

In more recent work, Sad, Neurock and Iglesia [35] showed that supported Cu catalysts together with minimal amounts of hydrogen produced via water gas shift reactions are also effective in the catalytic deoxygenation of alkanols, aldehydes, and alkane diols over dispersed Cu catalysts [35]. These reactions proceed via decarbonylation and decarboxylation paths. More interestingly, these reactions were also accompanied by C-C and C-O bond formation steps in what appear to be classic base catalyzed condensation and esterification pathways on the catalyst of Cu metal. Through rigorous kinetic analyses they were able to establish a network of deoxygenation, esterification and aldol condensation pathways (shown in Scheme 1) that result in the formation of the primary propylene, propane, propyl propionate and 3-pentanone products. The 3-pentanone product is thought to form via the reaction of a surface enolate with an adsorbed propanal intermediate to form the β-keto carbonyl intermediate which subsequently decarbonylates. The propyl propionate product, on the other-hand, is thought to be the result of Cu catalyzed esterification of two aldehydes similar to the classic base-catalyzed esterification routes proposed by Cannizaro and Tishchenko [36,37].

While previous kinetic studies carried out over $CuO/ZnO/Al_2O_3$ or Cu/ZnO [38] demonstrated aldol condensation of primary C_n alcohols to C_{2n-1} ketones, C-C bond formation was attributed to the basic ZnO support. The work of Sad, Neurock and Iglesia was the first to show that the Cu metal alone could catalyze the condensation as well as the esterification of equilibrium mixtures of propanol and propanal. They proposed that the unique Cu-catalyzed esterification and condensation pathways presented in Scheme 1 were the result of the in-situ formation of weakly held alkoxide intermediates on Cu that act as base to catalyze the C-C and C-O bond forming reactions. Detailed kinetic studies for the reactions of

equilibrium mixtures of propanal+H_2/propanol carried out at different temperatures showed that both esterification and condensation rates follow identical rate expression which suggests that the two reactions proceed either through the same rate determining step or via different reactions involving the same two reactive surface intermediates.
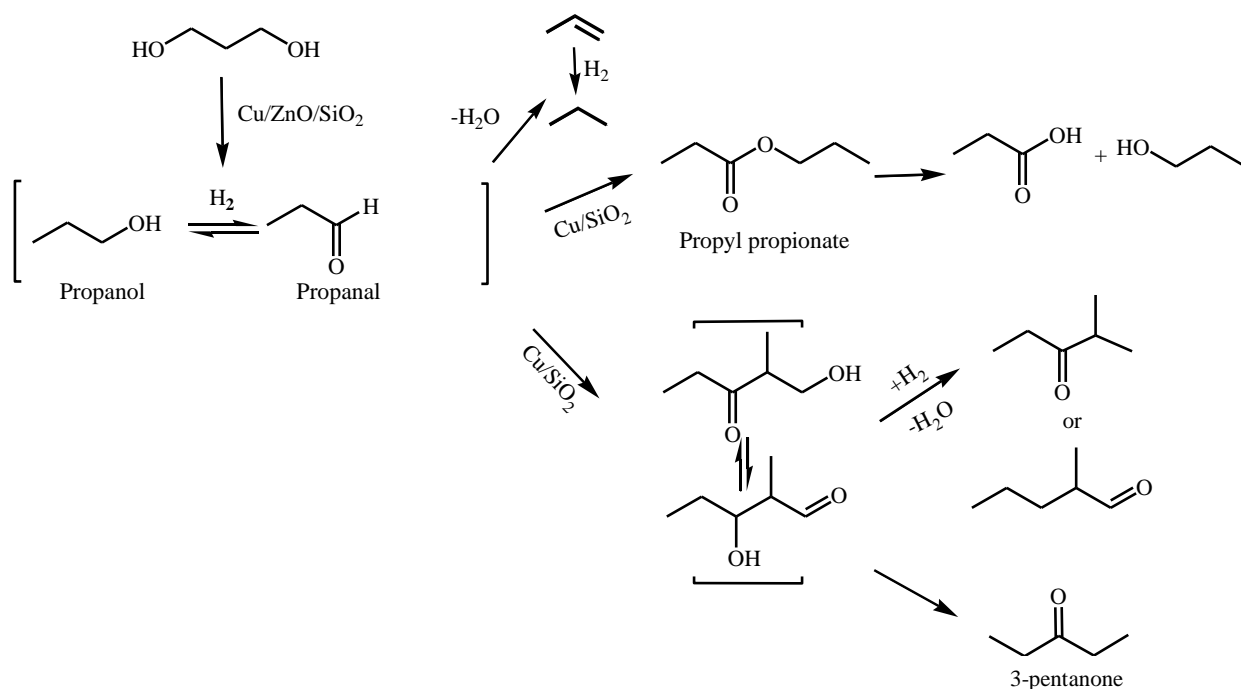
Scheme 1 The reaction network in our system. 1,3-dipropandiol is used as the initial reactant to be the model of polyol. By using Cu/ZnO/SiO$_2$ as catalyst, it is first converted to mixture of propanal and propanol. 3-pentanone and propyl propionate are the primary products from the equilibrated propanal and propanol in the environment of H_2, by using Cu/SiO$_2$ as catalyst. Reaction Condition: 10% wt. Cu/SiO$_2$ (5.5% dispersion). 503K. [35]

The turnover rates (TOR) for condensation were found to be a constant factor of two higher than those for esterification over a range of different propanol pressures [35]. In addition, the TOR decreased with increasing Cu dispersions which implied that the corner and edge sites bind the reactive surface intermediates to the metal surface too strongly thus increasing the activation barriers for both condensation and esterification. The most active surfaces appear to be those with larger fraction of low index planes.

While the previous kinetic data and rate laws provided invaluable insights into the possible mechanisms by which supported Cu metal can catalyze these base-catalyzed esterification and condensation pathways,

there is no direct information to support the proposed mechanisms or the catalytically active intermediates. Herein we have carried out a comprehensive set of first principle *ab initial* density functional theoretical calculations to analyze the mechanism by which the esterification and condensation pathways proceed over model Cu surfaces. We examine the elementary steps involved in the hydrogenation of propanal to propanol as well as the dehydrogenation of the propanol to propanal and hydrogen. The propoxide intermediate that forms was found to be rather basic on the Cu, and as such was found to catalyze the esterification and condensation pathways.

This thesis is organized as follows. The computational methods used to carry out all of the calculations reported in this work are described in Chapter 2. Chapter 3 examines the elementary steps involved in the equilibration of propanal and propanol, and the basicity of alkoxide that forms. The activation of the C-H bonds in the alcohol and aldehyde over the Cu metal surface as well as by the adsorbed alkoxide intermediates is discussed in Chapter 4. The C-C and C-O bond formation paths that result in aldol condensation and esterification are also presented in Chapter 4. Finally, Chapter 5 presents the conclusions from this work and recommendations for future studies.

Chapter 2 Methods

All of the calculated adsorption energies, reaction energies and activation barriers reported in this work were carried out using periodic plane wave density functional theory (DFT) calculations within the generalized gradient approximation using the Vienna *ab initio* Simulation Package (VASP) code [39]. The wave functions were represented by a series of plane wave basis functions expanded out to an energy cutoff of 396 eV using the Perdew-Wang form of the generalized-gradient approximation (PW91) [40]. The electron-ion interactions were described through the use of Vanderbilt ultrasoft pseudopotentials [41]. The surface Brillouin zone was sampled with a $3 \times 3 \times 1$ Monkhorst–Pack k-point grid. The electronic energies were converged to within $1*10^{-6}$ eV.

The Cu(111) surface was modeled using a four-layer slab comprised of 18 Cu atoms per layer in a (3×6) surface unit cell. A vacuum region of 10 Å was included between metal slabs to prevent any interactions between the slabs. During structure optimization for the Cu substrate with or without adsorbates, the bottom two layers of the Cu substrate were held fixed at the optimized positions for bulk Cu with Cu-Cu distance of 2.55 Å throughout the optimization. All of the remaining Cu atoms as well as all of the other atoms from the different adsorbates on the surface were optimized in all of the structural optimizations of the reactant, intermediate and product states. All of the optimized structures were converged within a tolerance of less than 0.05 eV/Å for relaxed degree of freedom.

The adsorption energies of stable gas phase molecules as well as the binding energies for unstable gas phase intermediates bound to the Cu(111) surface were calculated as:

$$\Delta E_{Ads} = E_{Adsorbates/Surface} - E_{Surface} - E_{Adsorbates} ,$$

2.1

Where $E_{Adsorbates/Surface}$ is the total energy of periodic metal surface together with the bound adsorbates, $E_{Surface}$ is the energy of clean Cu(111) surface, $E_{Adsorbates}$ is the energy of isolated and optimized gas-phase species.

The activation barriers were determined by using a two step transition state search scheme. The first step uses the nudged elastic band (NEB) method [42-44] to optimize the structures and corresponding energies for a sequence structures taken at equal distances along the minimum energy path. Each of these images were initially optimized until their forces normal to the reaction coordinate were calculated to be less than 0.25 eV/ Å. The highest energy image along the minimum energy path was subsequently chosen in order

to establish a first guess at the initial transition state structure which was used in Dimer method [45,46] to walk uphill along the reaction path in order to provide a more refined transition state (TSs) for a given elementary reaction step.

The reaction energies reported herein are calculated as the difference between the isolated product states minus the energy of the most stable reactant states. Similarly, the intrinsic activation energies are calculated as the difference between the isolated transition state and the corresponding most stable reactant state, while the overall activation barriers are calculated relative to the reactant state used initially as starting point for the reaction path.

The lowest energy reactant and product states were all calculated as isolated species on metal surface in order to explicitly remove the lateral interactions that occur between the co-adsorbed species. As such the reaction energy is then the difference in the summation of the total energies for each product species minus the summation for the total energies for reactant species as is shown in Eq. 2.2

$$\Delta E_{rxn} = \Sigma \ E_{Product \ i/Metal} - \Sigma\Delta E_{Reactant \ i/Metal} \hspace{3cm} 2.2$$

where $E_{Product \ i/Metal}$ refers to the total energy for isolated product species i adsorbed on the Cu(111) surface and $E_{Reactant \ i/Metal}$ refers to the total energy for isolated reactant species i on the Cu(111) surface. As an example, the reaction of A* + B* $\longrightarrow$ C* + D* would result in:

$$\Delta E_{rxn} = \ (E_{D/Metal} + E_{C/Metal}) - (E_{A/Metal} + E_{B/Metal}) \hspace{2cm} 2.3$$

where $E_{i}/_{Metal}$ refers to the total energy of species i on the bare Cu(111) surface. As the individual energy terms $E_{i}/_{Metal}$ refer to absolute energies from the calculations, we must be sure to include the total energy of the bare metal surface for reactant or product energies, for reactions which involve fewer reactants than products or fewer products than reactants, respectively. As such, the reaction energy for the following reaction A* + B* $\longrightarrow$ C* + *, would be:

$$\Delta E_{rxn} = \ (E_{C/Metal} + E_{Metal}) - (E_{A/Metal} + E_{B/Metal}) \hspace{2cm} 2.4$$

where E_{Metal} is the total energy of the bare Cu(111) surface.

The activation barriers were calculated similarly as:

$$\Delta E^* = E_{TST} - E_{reactant\ i/Metal} \qquad\qquad 2.5$$

for systems in which there is no loss in the number of species in going from the reactant to the product and:

$$\Delta E^* = (E_{TST} + E_{Metal}) - (E_{reactant\ 1/Metal} + E_{reactant\ 2/Metal}) \qquad\qquad 2.6$$

for systems in which two reactants combine to form the transition state.

The charges for reactant, product and transition states were carried out by using quasi-atomic minimal basis set orbitals (QUAMBO) [47,48], which construct highly localized quasiatomic minimal basis orbitals, based on geometries obtained initially using VASP package.

Chapter 3 Equilibrium between Propanal and Propanol

1,3-propandiol is used herein as a model polyol that is converted to the mixture of propanal and propanol in equilibrium with each other in the presence of H_2, over $Cu/ZnO/SiO_2$ catalyst as appears from the results presented in Scheme 1. The reactions of both propanal and propanol appear to undergo chain length growing reactions in the form of aldol condensation and esterification reactions, over Cu/SiO_2.

In this next section we discuss the equilibrium between propanal and propanol in the presence of H_2. The adsorption structure and energy of the surface propoxide, which is the key intermediate for the inter-conversion between propanal and propanol, is also analyzed here.

3.1 Equilibrium between propanol and propanal

Alkanols can dehydrogenate to form aldehydes and hydrogen over Cu at low temperatures [49]. This reaction is thought to proceed via the formation of an alkoxide intermediate. Steinrück *et al* [49], for example, showed that methanol adsorbs at 100 K on the Cu(110) surface and reacts at 200 K to form methoxy intermediates. Methoxy species was also reported as an intermediate that is formed in the oxidative dehydrogenation of methanol to formaldehyde over Cu surface [50-55]. The initial activation of methanol to methoxy occurs at ambient temperature, resulting in rapid equilibrium [56]. Similarly, the alkoxide intermediate can be formed via the reverse reaction which involves the hydrogenation of the aldehyde to the alkanol [57].

In order to examine the dissociation of the alkanol to form the aldehyde with hydrogen and the microscopic reverse reaction, we first examine the lowest energy adsorption states of alkanol and the aldehyde over Cu. As was reported above all of the studies will focus on the reactions of propanol/(propanal +H_2) over the Cu(111) surface.

The different adsorption configurations and energetics of propanol and propanal on Cu(111) are reported in Table A1.1 and Table A1.2 in the Appendix. Propanol adsorbs most favorably atop a Cu atom center but tilts slightly with respect to the surface (see FigA1.2 (e) in Appendix) which is consistent with other theoretical results for the adsorption of methanol [58,59] on Cu as would be predicted from valence shell electron pair repulsion model. The adsorption energy for propanol at the atop position is 35 kJ/mol. All of the other configurations initially examined were at least 17 kJ/mol less stable. Propanal also adsorbs atop a Cu metal atom through its oxygen resulting in an adsorption energy of 18 kJ/mol, therefore indicating a relative weak adsorption on Cu surface, consistent with previous reported results [58].

The dehydrogenation of propanol to form propanal requires the activation of both the O-H and the C-H bonds from the terminal hydroxyl carbon. This can proceed either by the initial activation of the O-H bond to form the alkoxide or via the C-H bond to first form the hydroxyl intermediate. The barrier to activate the O-H bond first to form the alkoxide is calculated to be 120 kJ/mol (Fig 3.1). The subsequent activation of the C-H bond was calculated to have a very similar intrinsic barrier at 117 kJ/mol. The overall barrier measured with respect to the most stably adsorbed propanol is 135 kJ/mol. However, if the C-H bond is cleaved first, the intrinsic C-H activation energy is significantly higher at 143 kJ/mol. The activation of the subsequent O-H bond has an overall barrier with respect to most stable adsorption of propanol at 163 kJ/mol. It is clear from the comparison of the reaction coordinate diagrams for both paths which are shown in Fig 3.1 that propanol dehydrogenation proceeds via the initial activation of the O-H bond to form the propoxide ($CH_3CH_2CH_2O*$) intermediate rather than the initial activation of C-H bond to form the hydroxyl propyl (CH_3CH_2C*HOH) intermediate. This is consistent with reported experimental results which indicate that Cu activates the O-H bond of methanol [56].

As a result of microscopic reversibility, the reverse reaction involving the hydrogenation of propanol to propanal, proceeds through the same transition state. The barrier for this step is only 56 kJ/mol from the adsorbed propanal state. The barriers for the subsequent formation of the alkanol were calculated to be 102 kJ/mol from the adsorbed alkoxide and only 41 kJ/mol from the most stably bound propanal. The propanol dehydrogenation and the propanal hydrogenation reactions examined here were found to be in rapid equilibrium with one another and as such are treated as indistinguishable species regarded as the "reactant pool" [35].
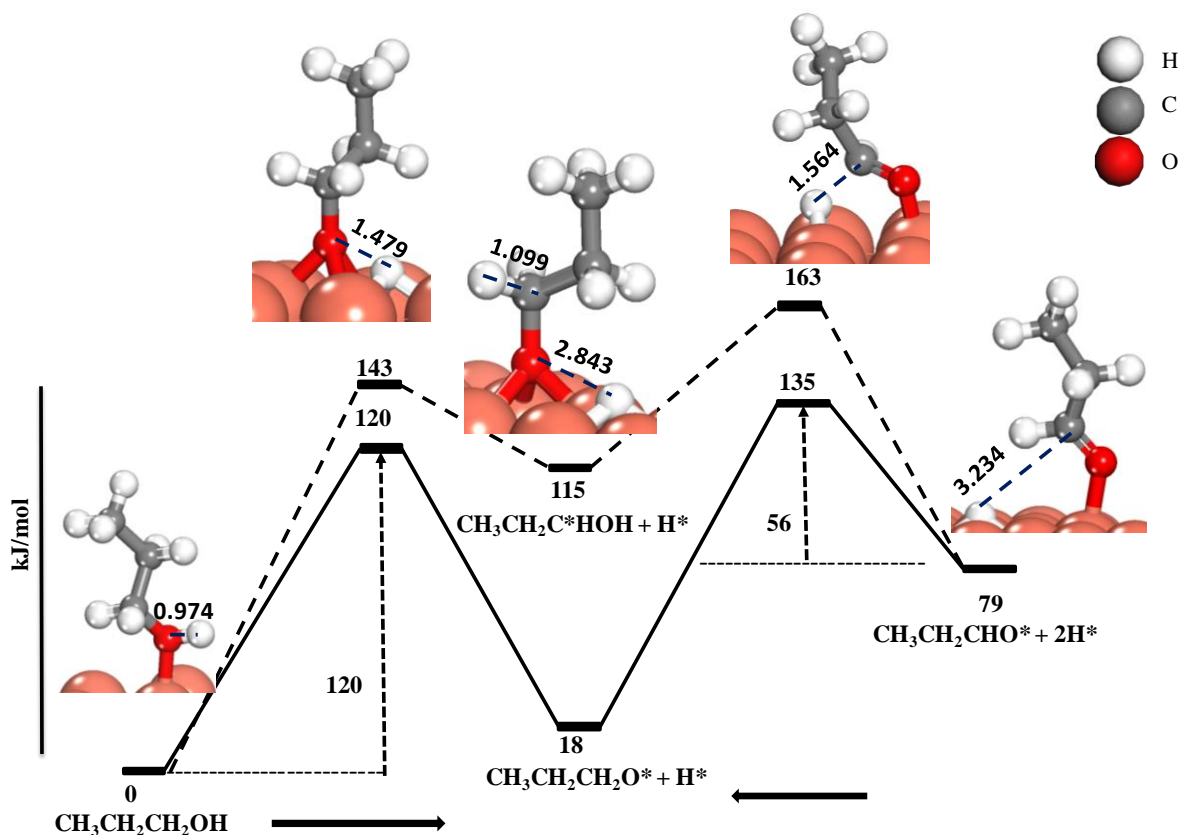
Fig 3.1 Pathways for the interconversion between propanol and propanal

Another point in Figure 3.1 that is worth noting is that the activation of the C-H bond on the carbon adjacent to oxygen atom is easier to activate for propoxide (117 kJ/mol) than that for propanol (143 kJ/mol). This provides further evidence that the most favorable path for the activation of propanol to propanal proceeds via the initial activation of the O-H bond to form the alkoxide rather than the activation of C-H bond [60].

Chapter 4 Reaction of Propanal and Propanol

Previous results reported by Sad *et al.* [35] showed that equilibrated mixtures of propanol-propanal-H_2 can be catalytically converted at 503 K over supported Cu catalysts to a range of different products from deoxygenation via hydrogenolysis, esterification and aldol condensation reaction pathways as was shown in Scheme 1. The major products that result from these reactions are 3-pentanone and propyl propionate, which are derived from aldol condensation and esterification paths, respectively. Small amounts of propane and propene as well as 3-methyl-pentanone were also formed likely as a result of hydrogenolysis and aldol condensation paths respectively [35].

The classic mechanisms for aldol condensation and esterification are shown in Scheme 4.1. Aldol condensation proceeds via a base catalyzed activation of the acidic α-C-H bond of an aldehyde or ketone to form an enolate intermediate. The enolate subsequently undergoes a nucleophilic attack at the carbon of another aldehyde or ketone to form the β–hydroxy carbonyl intermediate (aldol). Further dehydration of the aldol would result in the α,β - unsaturated aldehyde. Esterification, on the other hand proceeds via the nucleophilic attack of the basic alkoxide at the carbon atom of a second carbonyl to form an ester.

STEP1: Formation of Aldol

STEP2: Dehydration to
α,β - unsaturated aldehyde

(a) Aldol Condensation
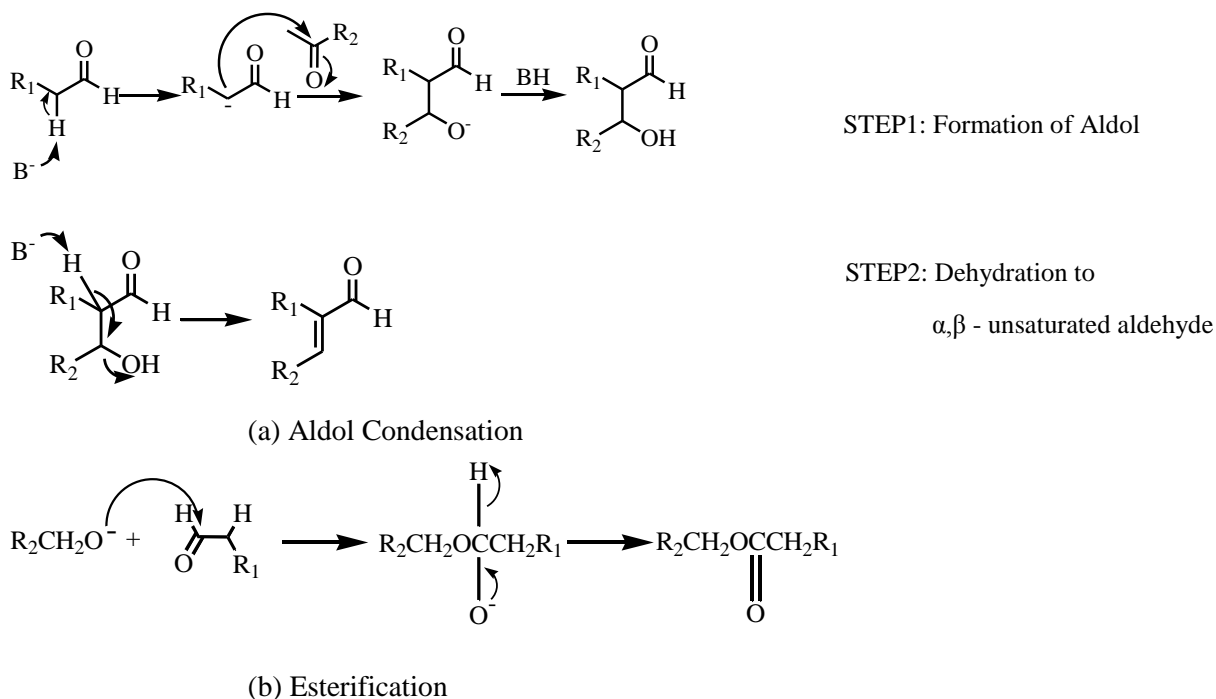
(b) Esterification

Scheme 4.1 Mechanism of base catalyzed (a) aldol condensation and (b) esterification.

Both aldol condensation and esterificaiton reactions are well established base-catalyzed reactions. The experiments reported by Sad *et al.* [35], however, were carried out over Cu/SiO_2 in gas phase and in the absence of a base. These reactions were suggested to be catalyzed by the "in-situ" formation of surface alkoxide intermediates which can take on base character when adsorbed on group IB metals as a result of their weak interaction with the surface. In the following section, we probe the electronic structure and characteristic of the propoxide intermediate that forms on Cu(111) surface.

4.1 The basicity of *OR on Cu surface

A base can be characterized by its ability to donate electrons [61]. Alkoxy anions (RO^-) in solution are known to be rather basic as they can effectively abstract protons or readily catalyze nucleophilic attack. Alkoxide intermediates (*OR) bound to group 1B metals may act to polarize a significant degree of electron density from the metal and thus begin to mimic the electronic character of the anionic solution phase alkoxides. The DFT-calculated electron density for the propoxide adsorbed on Cu(111) surface is shown in Fig. 4.1 and quantitatively presented in Table 4.1. The left picture in Fig. 4.1 shows that the propoxide is adsorbed via its oxygen to a three-fold Cu site with its CO axis normal to the metal surface with an adsorption energy of 218 kJ/mol. The three copper atoms connected with the oxygen are labeled as Cu1, Cu2 and Cu3. The picture on the right hand side in Fig 4.1 depicts the charge differences calculated using QUAMBO on the local Cu atoms and the alkoxide that occurs upon the adsorption of the alkoxide to the Cu surface. As indicated in the image, there appears to be a significant shift in the electron density from the Cu metal onto the oxygen upon adsorption.

The calculated charges on each of the atoms involved in the Cu-alkoxide complexes are reported in Table 4.1. The results show a significant increase of electron density on the oxygen atom upon adsorption and a concomitant loss of electron density on the local copper atoms. The charge on the oxygen atom increases by 0.5e- (from -2.33e- to -2.83e-) upon the adsorption of the propoxide intermediate onto the Cu(111) surface. This transfer of electrons from Cu into the adsorbed alkoxide increases the basicity of the alkoxide allowing it to behave similar to that of the negatively charged propoxide intermediate that carries out basic reactions in solution. As a comparison, we examine this same charge density difference analysis for propanol in the gas phase and adsorbed on the Cu(111) surface. The results reported in Table 4.1 indicate that there is no charge transfer from the Cu to the oxygen in propanol. As such, adsorbed propanol does not take on base character upon adsorption onto Cu.
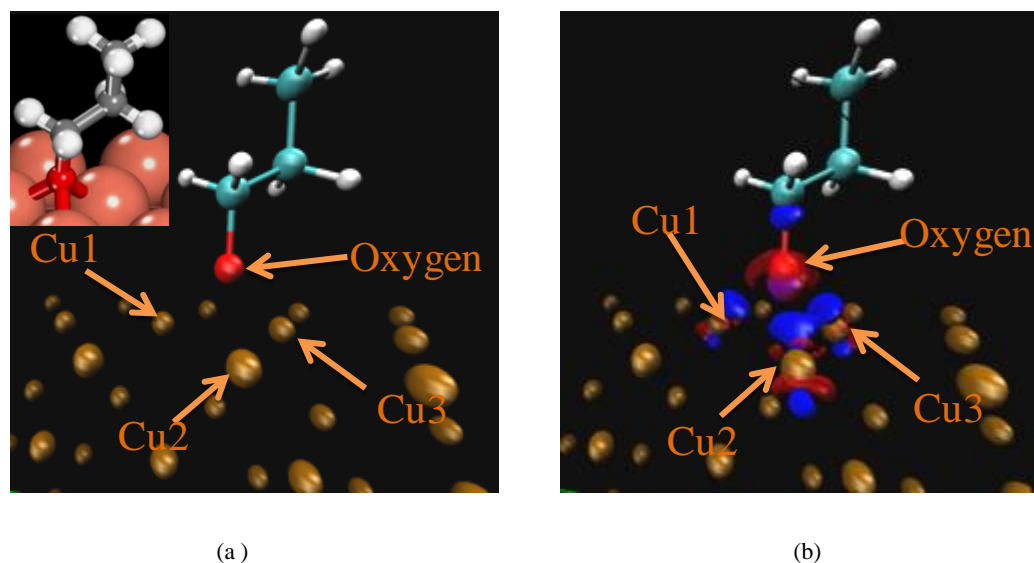
(a)　　　　　　　　　　　　　　　　　(b)

Fig 4.1 The example of charge difference analysis for alkoxide on Cu. (a) The adsorption configuration of alkoxide on Cu (3-fold site); (b) The charge density difference between the adsorbed alkoxide and the alkoxide in the gas phase. The red isosurface depicts an increase of charge density whereas the blue isosurface reveals a decrease of charge density.

Table 4.1 Charge difference analysis of oxygen in alkoxide and alcohol before/after adsorption [a]

Species	Before Adsorption (e⁻)	After Adsorption (e⁻)
Cu1	0.06	0.25
Cu2	0.04	0.22
Cu3	0.03	0.24
Oxygen in alkoxide	-0.33	**-0.81**
Oxygen in alcohol	-0.62	**-0.62**

(a) The charge difference analysis is carried out by QUAMBO

In previous studies [62], we have shown that adsorbed hydroxyl species (*OH) on the Au(111) surface also pick up electron density from the Au atoms. The *OH behaves as a base that decrease the barriers for O-H and C-H bond activation of the terminal hydroxyl group of alcohol intermediate to form the resulting aldehyde [62]. These adsorbed hydroxyl intermediates (*OH) were also found to undergo a nucleophilic attack on the carbonyl group of the aldehyde to produce carboxylic acid. A comparison of the charges on the O atoms for *OH and *OR species adsorbed on different metal surfaces is helpful in understanding the relative basicity of the two.

The extra electron density that resides on the oxygen atom for *OH adsorbed on different transition metals range from -0.33 to -0.66 e⁻, with the greatest electron density occurring for the group IB metals (Cu, Ag, and Au) as is shown in Table 4.2. Similarly, the extra negative charge on the oxygen atom for *OR on different metals was calculated to be ranging from -0.22 to -0.48 e⁻ with Cu, Ag, and Au, showing the greatest degree of charge transfer. The increase in the charge on the oxygen indicates an increase in the basicity of the adsorbed *OH or *OR intermediate. The reactivity of the *OH intermediate in abstracting acidic hydrogen from O-H and C-H bonds of adsorbed alcohols and aldehydes, as well as its reactivity with electrophilic C=O bonds [62], also provides direct insights into the basicity of the *OH adsorbed on model Au and other transition metal surfaces. The results presented herein as well as in previous studies clearly show that both *OR and *OH groups bound to the surface of coinage metals (group IB, including Cu, Ag and Au) are basic as the oxygen picks up significant electron density from the metal surface, as shown in Table 4.2. The charges transferred to the *OR and *OH species from other metals are significantly less than that from group IB metals. This is due to the fact that the d-bands of the coinage metals are nearly fully occupied (Cu: $3d^{10}$; Ag: $4d^{10}$; Au: $5d^{10}$) and as a result electrons will readily transfer out of these states and over to the adsorbed *OR or *OH intermediates.

Table 4.2 Summary of the charge accumulated on O atom for adsorbed *OH and *OR group

Species	Metal	Charge on O after adsorption	Species	Metal	Charge on O after adsorption
*OH (-0.44) [a]	Cu	-1.05	*OR (-0.33) [a]	Cu	-0.81
	Au	-1.04		Au	-0.77
	Ag	-1.07		Ag	-0.81
	Pd	-0.79		Pd	-0.56
	Ru	-0.77		Ru	-0.54
	Rh	-0.77		Rh	-0.55

(a) The number in the bracket is the extra charge for OH/OR group before adsorption

4.2 C-H activation of Propanal and Propanol

The enolate which is the key intermediate involved in aldol condensation shown in Scheme 4.1 forms as a result of the abstraction of the α-hydrogen of propanal. As propanal and propanol are equilibrated, we also examine the activation of the C_α-H bond of propanol for comparison. Considering the basicity of

alkoxide and the acidity of C-H at the α position of aldehyde, the adsorbed *OR would be expected to help activate the C-H bond.

4.2.1 C-H Activation of Propanal

The different adsorption configurations and the corresponding energies of C-H activated species of propanal are shown in Appendix, Table A1.1. The adsorption energies for all these intermediates were calculated to be between 144-159 kJ/mol. Especially, enolate, which is an alkyl surface intermediate (CH$_3$C*HCHO), is the result of the activation of the α-C-H bond (C$_\alpha$-H) of an aldehyde.

The activation of the C$_\alpha$-H bond solely over Cu sites on the Cu(111) results in the formation of a hydrogen atom and the propoxide product that preferentially bind to the three-fold Cu site and atop a vicinal Cu atom, respectively. The activation of the C$_\alpha$-H bond by an adsorbed *OR intermediate, however, proceeds via a proton abstraction by the alkoxide to form the HOR alcohol from the bounded alkoxide. These metal and alkoxide catalyzed C-H activation processes are depicted in Scheme 4.2 (a) and (b), respectively.

(a)   (b)
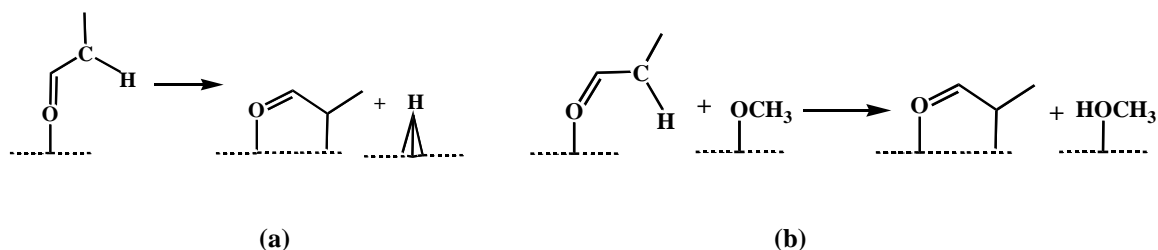
Scheme 4.2 The activation of the C-H bond of propanal can be catalyzed by either (a) the metal surface or (b) the adsorbed alkoxide (*OR) (Herein we use the -OCH$_3$ intermediated to simplify our calculations). The activation of C-H at **α** position is taken as an example.

For illustration purposes we define the carbon atom in the carbonyl group as C$_{car}$, the carbon atom at the α position of carbonyl group as C$_\alpha$ and the carbon atom of the terminal CH$_3$ group as C$_{end}$. The C-H bond on relevant carbon atoms are C$_{car}$-H, C$_\alpha$-H and C$_{end}$-H. Comparisons of the activation barriers (E$_a$ (C$_\alpha$-H) = 91 kJ/mol vs. E$_a$ (C$_{end}$-H) =156 kJ/mol), as well as the overall reaction energies, indicate that the activation of the C-H bond at the C$_\alpha$ position is considerably more favorable than the activation at the C$_{end}$. C-H bond activation at the C$_\alpha$ position results in the formation of an enolate intermediate, which is stabilized by resonance over the C$_\alpha$ and the carbonyl group [63]. The barrier for the base (*OR) catalyzed activation of the C$_\alpha$-H bond was found to be only 57 kJ/mol, which is 34 kJ/mol lower than that for the metal catalyzed activation of the same bond. The activation of the C$_{end}$-H bond by the *OR intermediate,

however, was found to be 157 kJ/mol which is significantly higher than the barrier for the based catalyzed C_α-H path, as is shown in Table 4.3. The hydrogen at the C_α position of aldehyde was calculated to be considerably more acidic than the one located at the C_{end} position. The C-H bond at C_α position has a pKa of 16-20 while that at the C_{end} position was reported to be 40-50 [63]. Therefore, the results clearly indicate that the aldehyde is most readily activated via the adsorbed base (alkoxide) at the C_α-H position rather than the C_{end}-H position. The adsorbed *OR species also demonstrated lower barriers (higher activity) and higher selectivity than the clean metal to catalyze the C-H activation reaction. This is consistent with the experimental results [35], which suggest the preferential formation of 3-pentanone via classic aldol condensation path, instead of the formation of linear alkanal (hexanal) via C-H bond cleavage at the C_{end} position.

It should be noted that the adsorbed base (*OR) does not show any real enhanced activity for the activation of C_{car}-H bond. The presence of *OR was found to actually increase the barrier. The energy penalty to move it from the most stable three-fold site to less stable atop site during the process of approaching to the H atom of the carbonyl group contributes significantly to the increase of reaction barrier. This is consistent from previous theoretical calculations, which show that although the homolytic activation of the C_{car}-H ($E_a = 29$ kJ/mol) is easier than the C_α-H [35], the heterolytic H-abstraction from the carbonyl group of an aldehyde by –OH (g) in the gas phase is ~60 kJ/mol higher than that at the acidic α-position.

**Table 4.3** Reaction and Activation energies of C-H bond activation for propanal and propanol

Broken bond/condition	Reaction energy (kJ/mol)	Activation energy (kJ/mol)
Alkanal C-H of C_{car} / without OR	37	91
Alkanal C-H of C_α / without OR	40	91
Alkanal C-H of C_{end} / without OR	104	156
Alkanal C-H of C_{car} / with OR	22	122
Alkanal C-H of C_α / with OR	**34**	**_57_**
Alkanal C-H of C_{end} / with OR	89	157
Alcohol C-H of C_{car} / without OR	110	141
Alcohol C-H of C_α / without OR	109	162
Alcohol C-H of C_{end} / without OR	121	170

Alcohol C-H of C_{car} / with OR	99	162
Alcohol C-H of C_α / with OR	96	151
Alcohol C-H of C_{end} / with OR	109	159

4.2.2 C-H Activation of Propanol

In addition to the C-H activation steps of the propanal, we also systematically examined the C-H activation paths for the propanol. The calculated adsorption configurations and the corresponding binding energies for propanol and its activated intermediates are listed in Appendix, Table A1.2.

The results for the Cu-catalyzed C-H activation show that the C-H bond of the terminal –CH$_2$OH group is the most active as the -OH group withdraws electron-density from the C-H bond leading to an inductive effect as is shown in Schemed 4.3 which lowers the activation energy [63]. The activation of the other C-H bonds increase as their distance from the terminal –CH$_2$OH group increases. A detailed charge analysis shows that the C_{car} has an excess charge of -0.2 e$^-$, while C_α has an excess charge of -0.4 e$^-$ and the C_{end} has an excess charge of -0.6 e$^-$. In other words, the carbon which is adjacent to oxygen has the lowest charge density among the three carbon atoms, indicating the weakest C-H bond.

$$\overset{\delta^{+++}}{CH_3} \longrightarrow \overset{\delta^{++}}{CH_2} \longrightarrow \overset{\delta^{+}}{CH_2} \longrightarrow \overset{\delta^{-}}{OH}$$
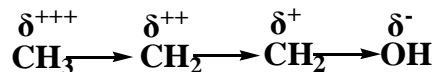
Scheme 4.3 Illustration of the electron-withdrawing inductive effect of hydroxyl group in propanol molecule. The amount of charges relative to the original charge of C: $\delta^+ > \delta^{++} > \delta^{+++}$. The arrow shows the direction the charges flows.

The trends for the activation of C-H bonds in propanol by *OR group are quite different than those reported above for propanal. The C-H activation barrier in propanol changes by only 11 kJ/mol in the activation of the C_{car}, C_α and C_{end} whereas the barriers for propanal change by 100 kJ/mol. The C_α-H bond of propanal is quite acidic and can be readily deprotonated to form a surface enolate species which delocalizes its negative charge over the C_α-CH=O group. Propanol lacks the presence of the neighboring C=O bond and the influence of conjugation to stabilize the negative charge that results upon the heterolytic activation of the C-H bond. As such, minor differences in the acidity of the C-H bonds of propanol help to explain the relatively high activation barriers required to activate the C-H bonds heterolytically as well as the weaker changes in barrier in changing the C-H bond than those reported for propanal.

In summary, the C-H bond activation preferentially proceeds via the adsorbed *OR which acts as a base and abstracts the most acidic hydrogen which is located at the α position of propanal to form an enolate

surface intermediate. This enolate intermediate can subsequently react with a second adsorbed aldehyde intermediate via aldol condensation to form a new C-C bond that increases the hydrocarbon backbone. The charge analysis result, as well as the higher barriers to activate the C_{end}-H, C_{car}-H bond in aldehyde or the C-H bonds in the alcohol, are consistent with the high selectivity to form C-C bonds solely at C_{α} position of aldehyde.

4.3 Aldol Condensation

The predominant intermediates that form from aldol-condensation are the β-hydroxyl and α,β-unsaturated aldehydes shown in Scheme 4.4a and 4.4b, respectively. The aldehyde reactants each of which are with n-carbons in length condense to form 2n carbon atom products. Other studies in the literature, however, indicate that the most favorable coupling products are comprised of 2n-1 carbon atoms [64,65] and suggest that aldol condensation is followed by a rapid decarbonylation or decarboxylation where oxygen is removed as either CO or CO_2, respectively as is shown in Scheme 4.4 c to d.

In order for the β-alkoxide intermediate to dehydrate to form the α, β-unsaturated alkanal (Scheme 4.4b), it may first undergo a hydrogen addition to form the β-hydroxy intermediate, shown in Scheme 4.4a. The β-alkoxide intermediate can also go on to form the decarbonylated/decarboxylated C_{2n-1} ketone, shown in Scheme 4.4d. This path however would more likely proceed via the dehydrogenation of the β-alkoxide intermediate to form the 2-formyl-3-pentanone (Scheme 4.4c) than via the hydrogenation. The 2-formyl-3-pentanone intermediate subsequently decarbonylates or decarboxylates to form the C_{2n-1} ketone.
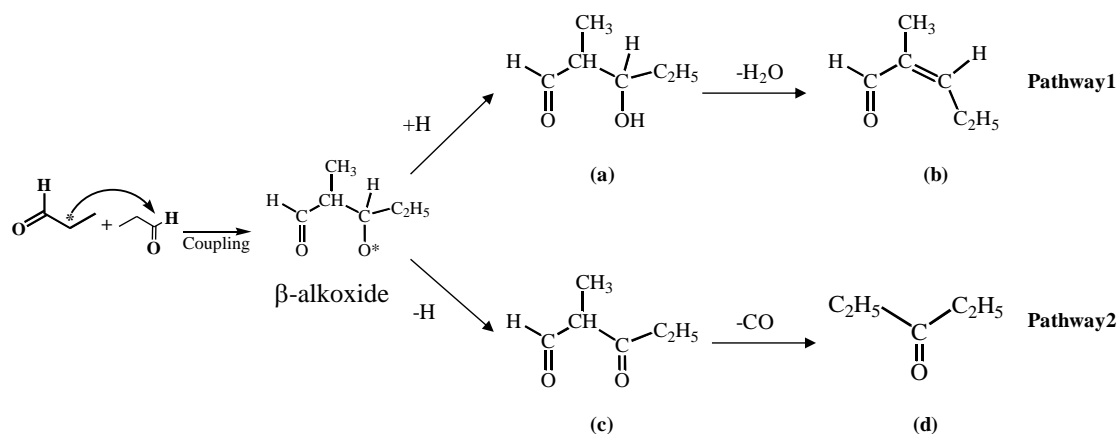
Scheme 4.4 Possible reaction pathways for aldol condensation. The reaction between propanal and its enolate can react via , (1) Pathway1 which proceeds through the dehydration of the β-hydroxy ketone intermediate to form the dehydrated C6 product shown in (b) and (2) Pathway2 which proceeds via a decarbonylation or decarboxylation path to C_5 product (3-pentanone).

Both the 2n-1 carbon product, 3-pentonone, and the 2n carbon products, 2-methylpentanal and 2-methyl-3-pentanone were detected experimentally [35]. The former product is the primary intermediate, whereas the later one has only been detected in limited amounts. As a comparison, Iglesia *et al*. [66] have shown that for Au/TiO$_2$, the formation of the 2n type product is significantly favored over the path to form 2n-1 type product. It is important to note that the reaction mechanism herein occurs solely on Cu metal surface with no influence from the support. The adsorption of all of the reactant, intermediate and product structures depicted in Scheme 4.4 are presented in the Appendix, Table A2.1 and Fig A2.1.

4.3.1 Formation of 2n type product

The condensation route to form C$_{2n}$ products presented as Pathway 1 in Scheme 4.4 proceeds through the nucleophilic attack of the enolate to the C=O bond of the adsorbed propanal to form the β-alkoxide aldol that subsequently hydrogenates to form the β-hydroxy aldol intermediate. The low barrier for the nucleophilic attack (9 kJ/mol) suggests that the enolate and the aldehyde species are very reactive. The subsequent hydrogenation of the β-alkoxide to form the β-hydroxyl intermediate has an apparent activation energy of 37 kJ/mol and an intrinsic barrier of 73 kJ/mol. The structures of reactants, products and transition states for both the coupling and hydrogenation steps are shown in Fig 4.2.

$CH_3CH_2CH=O* + CH_3C*HCH=O \longrightarrow CH_3CH_2CH(O*)CH(CH_3)CHO*$
$E_r = -36$ kJ/mol, $E_a = 9$ kJ/mol

$CH_3CH_2CH(O*)CH(CH_3)CHO* \longrightarrow CH_3CH_2CH(OH)CH(CH_3)CHO$
$E_r = -29$ kJ/mol, $E_a = 73$ kJ/mol
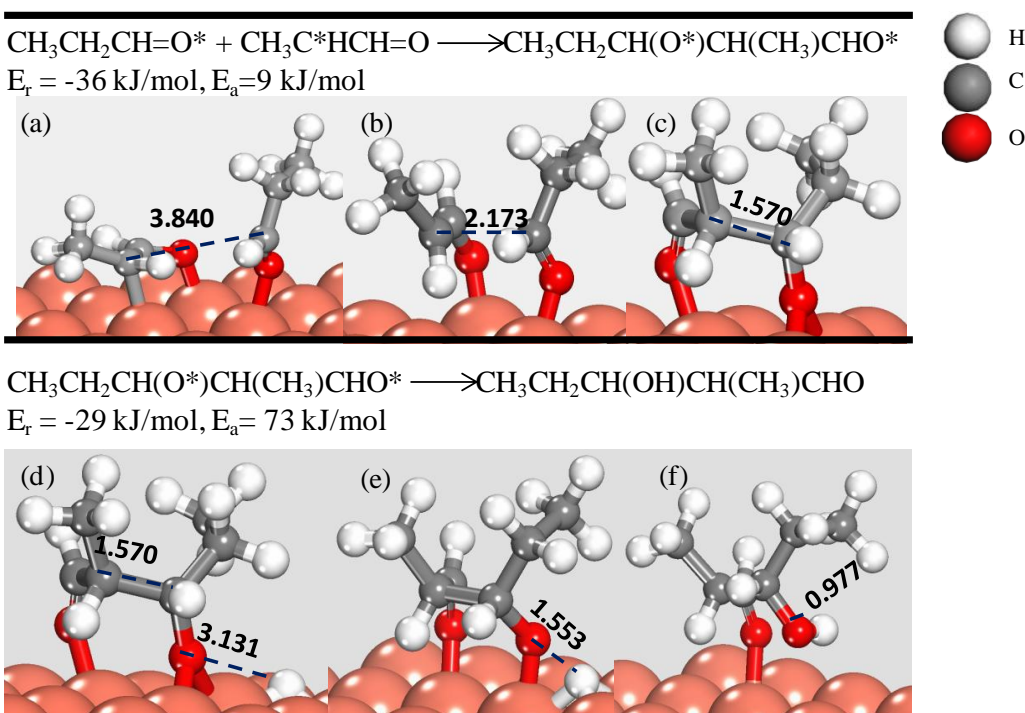
Fig 4.2 Structure of reactant, transition state and product states for the formation of β-hydroxyl product in aldol-condensation. (a)-(c) are for the coupling step. (d)-(e) are for hydrogenation step. E_r stands for reaction energy. E_a stands for activation energy.

The enolate intermediate adsorbs parallel to the Cu surfaces through its unsaturated C=C=O backbone and reacts with co-adsorbed propanal which is bound η_1 to the surface via its oxygen atom. The product of this reaction, $CH_3CH_2CH(O^*)CH(CH_3)CHO^*$ alkoxide-like intermediate shown in Fig. 4.2(c) that binds strongly (ΔE_{ads} = 208 kJ/mol) to the surface through both of its oxygen atoms. The addition of hydrogen to the internal oxygen results in the formation of the β-hydroxyl aldol $CH_3CH_2CH(OH)CH(CH_3)CHO^*$, shown in Fig 4.2 (f), which binds weakly to the surface via its terminal carbonyl with an adsorption energy of 36 kJ/mol.

4.3.2 Formation of 2n-1 type product

The paths that can result in the formation of the 3-pentanone product (2n-1 type) are shown in scheme 4.5. This reaction requires both C-C coupling and dehydrogenation, followed by the decarbonylation of the resulting alkoxide. We explore the energetics for initially proceeding via C-C coupling and subsequently carrying out dehydrogenation. In addition, we reverse these steps and examine dehydrogenation followed by C-C coupling.
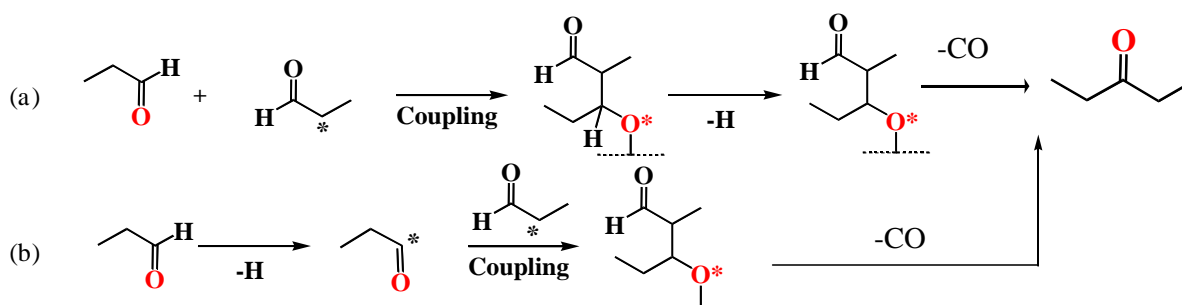
Scheme 4.5 The coupling of $CH_3C^*HCH=O$ enolate and propanal to form 3-petanone. (a) C-C coupling followed by dehydrogenation and (b) dehydrogenation followed by C-C coupling.

The coupling of the enolate ($CH_3C^*HCH=O$) with propanal ($CH_3CH_2CH=O$) proceeds via the nucleophillic attack of the enolate on the bounded C_{car} in propanal to form the $CH_3CH_2CHO^*$-$CH(CH_3)CH=O$ alkoxide intermediate, as depicted in Pathway (a) in Scheme 4.5, with a barrier of only 9 kJ/mol. This step was already analyzed as the first step in the 2n type mechanism shown in Figure 4.2a-c. The C-H bond of the adsorbed alkoxide can subsequently be activated to form the $CH_3CH_2CO^*$-$CH(CH_3)CH=O$ intermediate. This reaction can be carried out either by the metal or by an adsorbed alkoxide (*OR). The barriers that results for the C-H activation at the terrace, edge and corner sites of a metal cluster with metal coordination numbers of 9, 7 and 5, respectively are given in Table 4.4.

The results indicate that the barriers to activate the C-H bond by the terrace sites on Cu(111) surface or by adsorbed *OR are both rather high at 105 and 104 kJ/mol, respectively. The high barriers that result on the clean Cu(111) terrace are due to the high coordinative saturation of the Cu sites as well as the steric

interactions that result between the bulky CH$_3$CH$_2$CHO*-CH(CH$_3$)CH=O alkoxide intermediate and the coordinatively saturated metal sites in activating its C-H bond. The high barrier for the activation of the bound CH$_3$CH$_2$CHO*-CH(CH$_3$)CH=O intermediate by co-adsorbed *OR intermediates is due to the very weak acidity of the C(*O)-H bond, and the steric interactions that result between the adsorbed *OR and the CH$_3$CH$_2$CHO*-CH(CH$_3$)CH=O intermediate.

Table 4.4 activation energies for C-H cleavage during aldol condensation

Reaction Condition	Activation Energy (kJ/mol)
Cu(111) surface	105
Cu(111) surface + *OR	104
Step site on Cu surface	42

The barrier to activate this same C-H bond at a step site on Cu is only 42 kJ/mol and is significantly easier than the activation at the terrace site. The optimized structure of the CH$_3$CH$_2$CHO*-CH(CH$_3$)CH=O alkoxide at the step edge of Cu is shown in Fig 4.3. The lower barrier is the result of the coordinative unsaturation of Cu atoms at the top of the step edge and its ease of access to the C-H group as is shown in the transition and product states in Fig. 4.3.

CH$_3$CH$_2$CH(O*)CH(CH$_3$)CHO $\longrightarrow$ CH$_3$CH$_2$C(O*)CH(CH$_3$)CHO + H*

E$_r$ = 20 kJ/mol, E$_a$= 42 kJ/mol
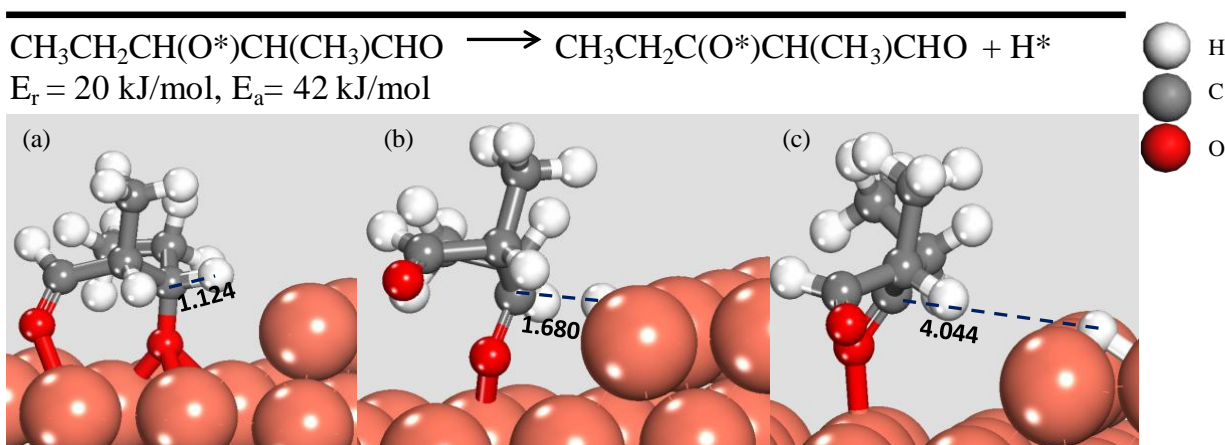
Fig 4.3 The (a) reactant, (b) transition state and (c) product of the C-H activation of the C-C coupling product on step site of metal surface.

If the C-H bond activation at C$_{car}$ of the propanal precedes the coupling between the enolate and propanal, the activation barrier to form the CH$_3$CH$_2$C*=O* intermediate (Pathway (b), Scheme 4.5) is 91 kJ/mol.

The overall barrier for the subsequent coupling of the $CH_3CH_2C^*=O^*$ and propanal is now 105 kJ/mol (intrinsic barrier is 72 kJ/mol).

Combining the calculated results above, it is clear that the path which proceed by initially carrying out C-C coupling followed by C-H activation (Fig 4.4) is much more favored than the path which proceeds via C-H activation followed by C-C coupling. The results here are consistent with the previous results discussed in Chapter 3 which indicate that the barrier to activate that C-H bond attached to the oxygen of an alkoxide is significantly easier than activating the same C-H bond of the corresponding alcohol. Therefore, the C-H activation occurs after the formation of the more reactive alkoxide, which is the result of the coupling between enolate and propanal. In addition, the barrier calculated for coupling the enolate and propanal (9 kJ/mol) is significantly lower than the barrier to couple the enolate and $CH_3CH_2C^*=O^*$ (68 kJ/mol). The lower barrier for propanal coupling is the direct consequence of the weaker adsorption of propanal on Cu (18 kJ/mol) over that of the $CH_3CH_2C^*=O^*$ species (159 kJ/mol) and thus the lower energy penalty required in breaking the Cu-C bonds in order to form the resulting C-C bond. As a result, the barrier necessary to couple enolate and propanal to form $CH_3CH_2CH(O)$-$CH(CH_3)$-$CH=O$ is lower. After coupling, the dehydrogenation step preferentially occurs at the more coordinatively-unsaturated edge or corner sites on the metal surface. The activation of the C-H bond of the $CH_3CH_2CH(O^*)$-$CH(CH_3)$-$CH=O$ intermediate results in a barrier that is 60% lower than on the pure metal surface even with *OR group present. This is subsequently followed by a decarbonylation step to form the final 2n-1 product. This later decarbonylation step is not specifically examined in the work discussed herein.
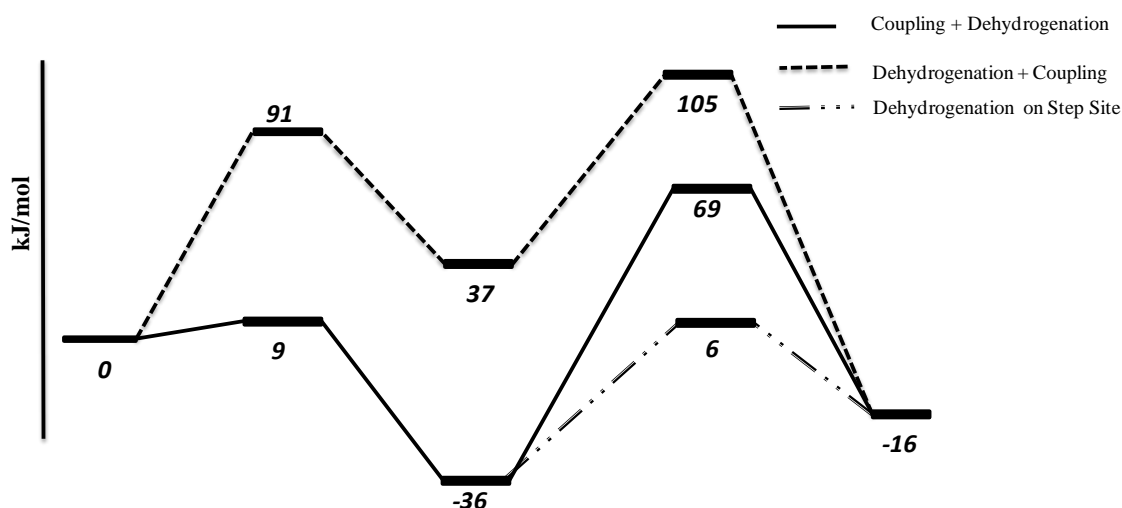

Fig 4.4 Comparisons of the reaction coordinates and energies required in carrying out the coupling and dehydrogenation steps and the relative order in which these two reactions proceed in aldol condensation.

4.3.3 2n type reaction vs. 2n-1 type reaction for aldol condensation

The 2n and 2n-1 type reactions have been studied in 4.3.1 and 4.3.2 sections separately and the first two steps for both reaction paths are shown in Fig. 4.5. Although, we did not specifically examine the final dehydration or decarboxylation/decarbonylation steps, the lower barrier for dehydrogenation of the enolate-propanal coupling product indicates the preference over the hydrogenation path. Experimental results also indicate that the reactions primarily produce 2n-1 type product.
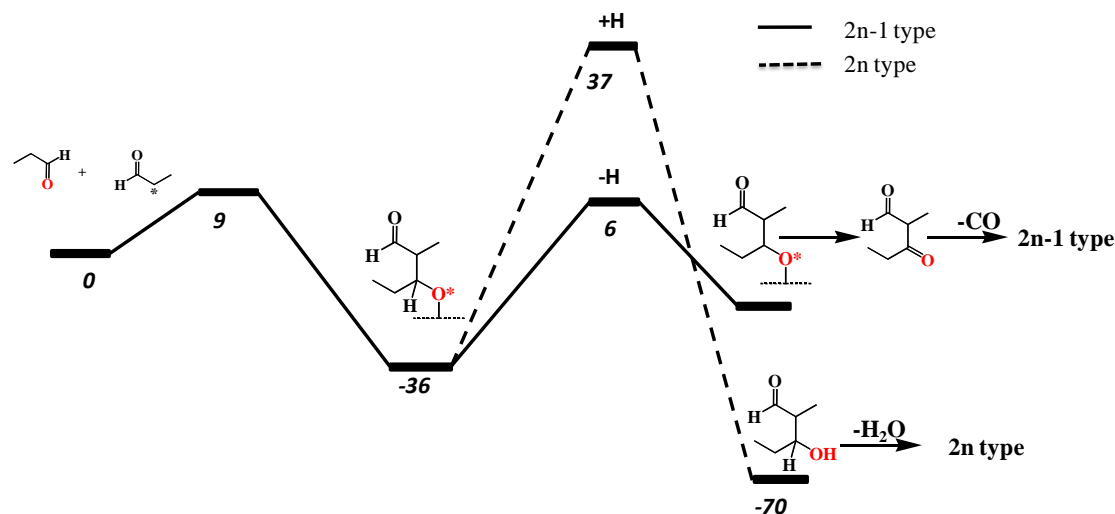
Fig 4.5 Comparison between (1) coupling + dehydrogenation and (2) coupling + hydrogenation pathways for aldol condensation.

Herein, we show the unique ability of monofunctional Cu metal to catalyze the preferential abstraction of hydrogen located at the α position of the aldehyde to form an enolate. The subsequent nucleophillic attack of the enolate to the adsorbed propanal results in C-C bond formation without the assistance of SiO_2 support. There is no experimental evidence for the formation of linear aldehydes, such as hexanal, which indicates that the activation of the C-H bond β to the carbonyl (C_{end} position) is difficult. Oxygen is subsequently removed from the aldol product via decarboxylation/decarbonylation rather than dehydration.

4.4 Esterification

Esterificaiton can occur by either acid or base catalyzed pathways. The acid route typically proceeds via the reaction between an alcohol and an acid with the elimination of water. The base-catalyzed route which we consider herein proceeds via the reaction between an aldehyde and an alcohol via the Tischenko reaction [37]. The reaction is thought to proceed via a nucelophillic attack of an alkoxide onto the carbon end of the carbonyl. In the reactions considered here the surface bound propoxide, formed from the O-H activation of the alcohol or the hydrogen-addition to the aldehyde, attacks an adsorbed surface propanal to form the $CH_3CH_2CH_2O\text{-}CH(O^*)CH_2CH_3$ alkoxide intermediate. C-O bond formation can also proceed through the nucleophilic attack of an acyl intermediate ($CH_3CH_2C^*{=}O^*$) to a second adsorbed aldehyde [35, 67, 68]. The $C_6H_{13}O^*$ or $C_6H_{11}O^*$ intermediate produced from these two possible pathways can dehydrogenate or hydrogenate, respectively to form the corresponding ester, as is shown in Scheme 4.6.

$$CH_3CH_2C^*{=}O^* \xrightarrow{CH_3CH_2CHO} C_6H_{11}O_2 \xrightarrow{+H} C_6H_{12}O_2 \qquad (a)$$

$$CH_3CH_2CH_2O + CH_3CH_2CHO$$

$$CH_3C^*HCHO \xrightarrow{CH_3CH_2CHO} C_6H_{13}O_2 \xrightarrow{-H} C_6H_{12}O_2 \qquad (b)$$
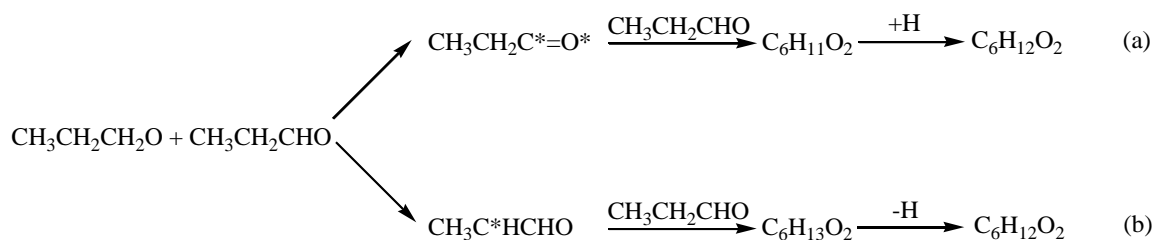
Scheme 4.6 Different esterification pathways (a) with $CH_3CH_2C^*{=}O^*$ as intermediate and (b) with CH_3CH^*CHO as intermediate.

The adsorption configurations for the reactant, intermediate and product molecules involved in the esterification of propanal and propanol and their corresponding adsorption energies are reported in Appendix A3. For the ester molecule, the most stable configuration is the one in which the oxygen in the carbonyl group adsorbs on metal surface with the adsorption energy of 31 kJ/mol.

If the esterification reaction proceeds via the coupling between propanal (CH_3CH_2CHO) and the acyl intermediate ($CH_3CH_2C^*{=}O^*$), as is shown as Path (a) in Scheme 4.6, the C-H bond at C_{car} is first activated in order to generate an initial acyl intermediate. In section 4.3, we showed that the barrier to abstract the H from the C_{car} position of propanal can have relatively high value, 91 kJ/mol. The $CH_3CH_2C^*{=}O^*$ intermediate is also much more strongly bound to the surface (159 kJ/mol) than propanal. This suggests that $CH_3CH_2C^*{=}O^*$ would not be involved in esterification process.

Instead, our theoretical results indicate that esterification preferentially proceeds via the coupling between alkoxide and propanal. Similar to paths for aldol condensation, esterification can first proceed either via coupling or dehydrogenation. If the coupling occurs first, nucleophillic attack of the adsorbed propoxide

to the carbon of the carbonyl group of adsorbed propanal has an activation energy of 53 kJ/mol. The subsequent dehydrogenation of the $CH_3CH_2CH_2O\text{-}CH(O^*)CH_2CH_3$ alkoxide can occur with activation energy of 57 kJ/mol at step site, or via a hydrogen abstraction by an adsorbed *OR species with a barrier of 88 kJ/mol, respectively. The very weak acidity of the C-H bond on the $CH_3CH_2CH_2O\text{-}CH(O^*)CH_2CH_3$ alkoxide, the repulsive interactions associated with the bringing in an adsorbed alkoxide to the sterically hindered alkoxide and the energy cost associated with moving the adsorbed *OR from three-fold site to atop site lead to the relatively higher barrier for hydrogen abstraction when *OR exists. In another case, the calculated barriers for both dehydrogenation and coupling were found to be significantly higher when dehydrogenation preceded the formation of the C-O bond, as shown in Fig 4.6.
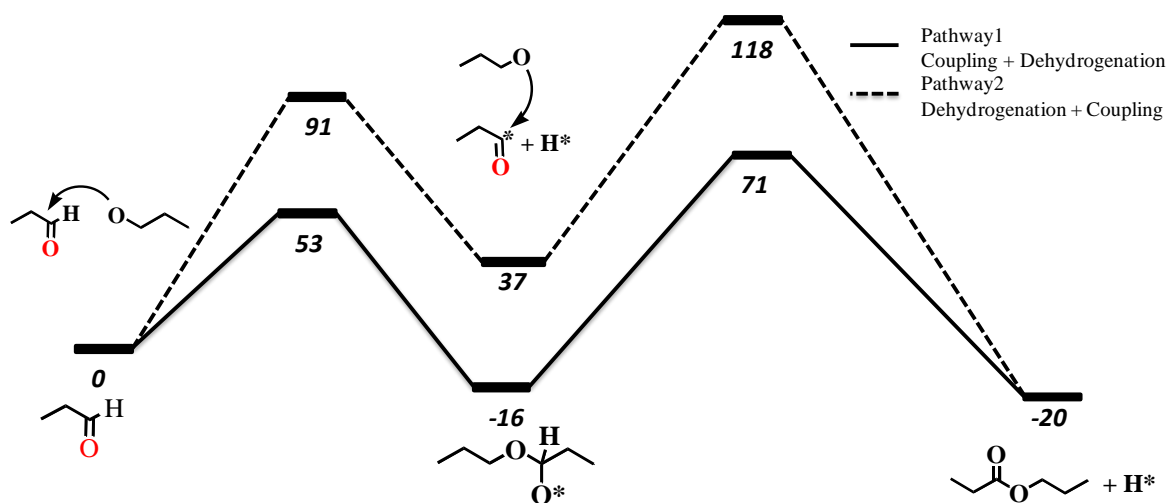
Fig 4.6 Reaction coordinate of esterification. In pathway 1, C-O bond formation preceeds dehydrogenation whereas in pathway 2, dehydrogenation preceeds C-O bond formation. The calculated values have units of kJ/mol. Pathway 1 which proceeds via C-O coupling followed by dehydrogenation appears to have lower activation energies for both C-O coupling and dehydrogenation.

A similar mechanism was previously reported for the esterification of methanol [69] and ethanol [70] over Au. In these reactions, the adsorbed atomic oxygen (O*) is used to activate the alkanol to form surface alkoxides, which subsequently react with adsorbed aldehyde. The C-H bond cleavage was shown to occur after the C-O bond is formed.

As a conclusion, the alkoxide was found to preferentially couple with the adsorbed propanal $(CH_3CH_2CHO^*)$ rather than that with the dehydrogenated propanal $(CH_3CH_2C^*=O^*)$. The esterification reaction is thought to proceed via a nucleophillic attack of the propoxide on the propanal to form the C-O

bond which is followed by the subsequent dehydrogenation to form the ester product. The configurations of the reactants, products and transition states are shown in Fig. 4.7.
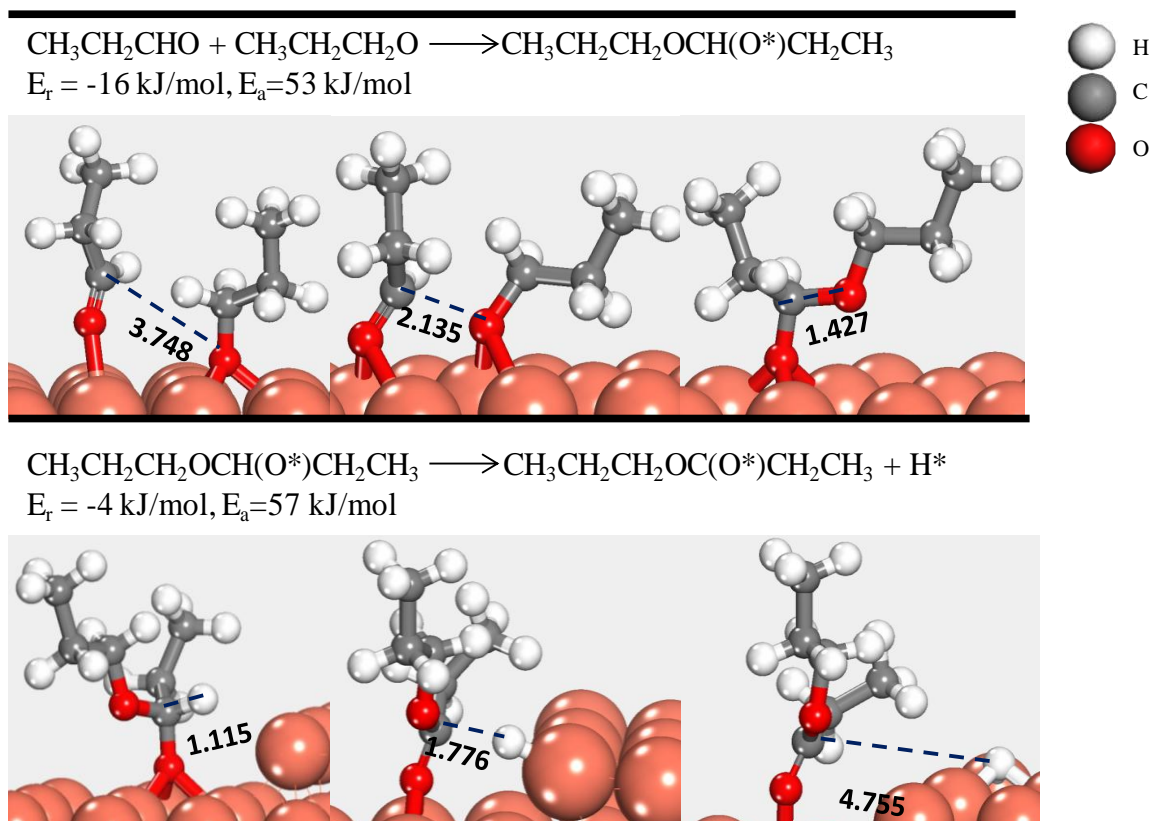
$CH_3CH_2CHO + CH_3CH_2CH_2O \longrightarrow CH_3CH_2CH_2OCH(O^*)CH_2CH_3$
$E_r = -16\,kJ/mol, E_a = 53\,kJ/mol$

$CH_3CH_2CH_2OCH(O^*)CH_2CH_3 \longrightarrow CH_3CH_2CH_2OC(O^*)CH_2CH_3 + H^*$
$E_r = -4\,kJ/mol, E_a = 57\,kJ/mol$

Fig. 4.7 Reactants, transition states and products for the esterification reaction over Cu(111). (a) - (c) are the relevant structures for C-O coupling step and (d) – (f) are the relevant structures for dehydrogenation on step site.

4.5 Comparison of condensation and esterificaiton

In order to compare the experimental data to our theoretical results, we analyze the reaction rates for esterification and condensation reported by Sad *et al.* [35] as shown in Fig. 4.8 together with the theoretical results reported herein. The experimental rates are determined as functions of measured propanal pressures. Both condensation and esterification rates appear to change in a very similar manner.

A quantitative comparison of the condensation/esterification rates versus propanal pressures, as shown in Fig.4.8, reveals that these two reactions have the same reaction orders and can be fit to the same kinetic expression shown in Eq. 4.1:

$$\upsilon = \frac{k_6^{"}}{K_3 \cdot K_4^2 \cdot K_5^{0.5}} \cdot \frac{[C_3H_6O]^2 \cdot [H_2]^{0.5}}{(1 + \frac{1}{K_4} \cdot [C_3H_6O] + \frac{K_1 \cdot K_2 \cdot K_5}{K_d} \cdot [C_3H_6O] \cdot [H_2]^{0.5})^2} \qquad \text{Equation 4.1}$$

which is derived from the elementary reaction steps. While the rate constants are different, the same form of the rate expression would indicate that the 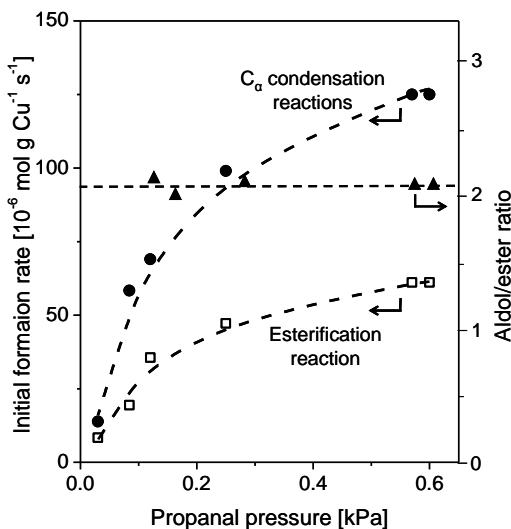kinetically relevant step in both reactions involve the same surface intermediates [35]. A closer analysis of the results also suggest that both of these reactions proceed by the reactions of adsorbed propanal ($CH_3CH_2CHO^*$) and surface propoxide ($CH_3CH_2CH_2O^*$).

Fig 4.8. Formation rate vs propanal pressure for esterification (□) and aldol condensation (●) reactions from propanol-propanal-H_2 mixtures on 10 % wt. Cu/SiO_2 (5.5% dispersion) in left axis. Aldol/ester ratio (▲) vs propanal pressure in right axis. [9]

This is consistent with the theoretical results illustrated in Fig. 4.9 which shows that the kinetic relevant steps in aldol condensation and esterification involve the H abstraction from the α position of propanal by the propoxide, forming the enolate intermediate (for aldol condensation) and the nucleophillic addition of the propoxide to the propanal (for esterification), respectively. As such, the rate controlling step in both systems involve the reaction between an adsorbed propoxide species and propanal.

The experimental results shown in Fig. 4.8 also indicate that the reaction rate for aldol condensation is a factor of two higher than that for esterification, over a wide range of propanal pressures [37]. By using the Arrhenius equation (Equation 4.2 and 4.3), we can estimate the difference between experimental activation energies of these two reactions.

$$r = A\exp(-E_a / RT) \qquad \text{Equation 4.2}$$

$$\frac{r_e}{r_a} = \frac{A_e \exp(-E_{ae} / RT)}{A_a \exp(-E_{aa} / RT)} = \frac{A_e}{A_a}\exp((E_{aa} - E_{ae}) / RT) \qquad \text{Equation 4.3}$$

r_e: rate for esterification; r_a: rate for aldol condensation; E_{ae}: activation energy for esterification; E_{aa}: activation energy for aldol condensation; A_e and A_a: pre-factor for esterification and aldol condensation. R=8.314 kJ/(mol*K)

Since r_a is two times that of r_e at reaction temperature (503K) from experimental results, this would indicate that the barrier for esterification is ~3 kJ/mol higher than that of aldol condensation (i.e. $E_{ae} - E_{aa} = 3$ kJ/mol).

Theoretical results for these two reactions, shown in Fig. 4.9, indicate that the barriers for aldol condensation and esterification are quite similar, but report instead that the barrier for condensation is 4 kJ/mol higher than that for esterification, which means $E_{ae} - E_{aa} = -4$ kJ/mol. Although the sign is different between experimental and theoretical estimations, the difference between these two is well within the accuracy of density functional theory of 10 kJ/mol.

In summary, the condensation and esterification reactions proceed by nucleophilic attack of enolate formed by an initial abstraction of the C_α hydrogen or alkoxide, to aldehyde, respectively. Dehydrogenation step follows subsequently. In the condensation reaction, the resulting aldol intermediate preferentially undergoes dehydrogenation, as opposed to hydrogenation, to form the $CH_3CH_2C(O)CH(CH_3)$-CH=O product that can subsequently decarbonylate generating 3-pentanone product which is consistent with experimental results.
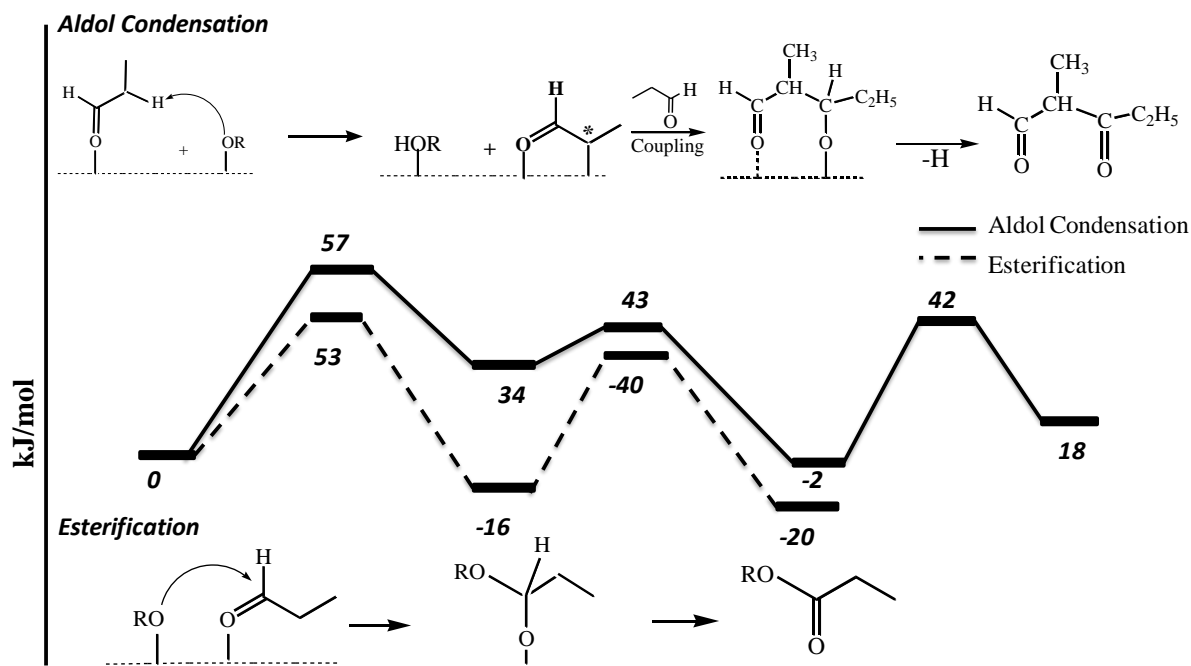

Fig 4.9 A more complete comparison between the energies for the elementary steps involved in aldol condensation and esterification reactions.

As the SiO_2 support does not show any activity to aldol condensation or esterification reactions in the experiment, the results indicate that Cu can catalyze these chain length growing reactions via the presence of the *OR basic promoter that is formed in-situ under reaction conditions.

Chapter 5 Conclusion

First principle density functional theory calculations have demonstrated that copper supported on silica is shown to catalyze both aldol condensation and esterification reactions and subsequent decarboxylation to remove oxygen, without the assistance of basic oxide support. With the equilibrated mixture of propanal-propanol-H_2 as reactant, the primary product for aldol condensation is 3-pentanone, which is sequentially produced by decarboxylation/decarbonylation after C-C coupling step. Classic aldol type products, such as 2-methyl-pentanal or 2-methyl-3-pentonone, which are derived from dehydration of β-hydroxyl carbonyl species, are detected in very little amount. Therefore, not only the chain length has grown with just a small barrier of 9 kJ/mol for C-C coupling, but also the oxygen content is decreased by using carbon resources within reactant molecule. At the same time, the valuable hydrogen is preserved within the oxygenates. Propyl propionate is another primary product under the reaction condition, demonstrating the ability of monofunctional Cu to catalyze the C-O bond formation.

Interestingly, aldol condensation and esterification shows similar dependence to reactant concentration and the Cu cluster size. Same rate equation formula is used to describe both of the reactions, pointing to the existence of similar kinetic relevant step. Alkoxide, the key intermediate in the inter-conversion of propanal-propanol, is demonstrated to be involved in both the abstraction of acidic α-H of aldehyde to produce surface adsorbed enolate in aldol condensation reaction, and the direct nucleophilic attack to vinyl adsorbed aldehyde, to form C-O bond in esterification reaction, respectively. Theoretical results show that both of these two steps have the highest activation energy in either condensation or esterification pathways, validating the nature of this alkoxide involved step to be the rate controlling kinetic relevant step.

Using charge analysis calculations we determined that oxygen atom in alkoxide accumulates extra charges. This fact render basicity to alkoxide that helps activate the acidic hydrogen situated at the α position of aldehyde with a barrier of 34 kJ/mol, lower than the situation without alkoxide. The hydrogen at the ending position of aldehyde is not easily activated, no matter whether the alkoxide species exists or not. Also, the alkoxide does not show preference to activate the C-H bonds in propanol.

Acknowledgements

Reference

[1] G. W. Huber, Sara Iborra, Avelino Corma, *Chem. Rev*. 2006, 106, 4044.

[2] J. N. Chheda, G. W. Huber, J. A. Dumesic, *Angewandte Chemie-International Edition.* 2007, 46,7164.

[3] A. Corma, S. Iborra, A. Velty, *Chem. Rev.* 2007, 107, 2411.

[4] A. V. Bridgwater, *Appl. Catal. A.* 1994,116,5.

[5] M. Snare, I. Kubickova, P. Maki-Arvela, K. Eranen, J. Warna, D.Yu. Murzin, *Chemical Engineering Journal*. 2007,134,29–34.

[6] Z.P.G. Masende, B.F.M. Kuster, K.J. Ptasinski, F.J.J.G. Janssen, J.H.Y. Katima, J.C. Schouten, *Appl. Catal.B.* 2005, 2005,189–199.

[7] D. C. Elliott, D. Beckman, A. V. Bridgwater, J. P. Diebold, S. B. Gevert, Y. Solantausta, *Energy Fuels*.1991,5,399.

[8] Furimsky, E, *Appl. Catal. A.* 2000, 199, 147.

[9] R.R. Davda, J.W. Shabaker, G.W. Huber, R.D. Cortright, J.A. Dumesic, *Appl. Catal. B: Env.*2005,56, 171.

[10]M. Stocker, *Angew. Chem. Int. Ed*. 2008, 47, 9200 – 9211.

[11] A. Demirbas, *Fuel.* 1998,77,1117.

[12] I. Kubickova, M. Snåre, P. Maki Arvela, K. Eranen, D. Yu Murzin, *Catal. Today.* 2005, 106,197.

[13] M. J. Overett, R. O. Hill, R. John Moss, *Coordination Chemistry Reviews.* 2000,206-207, 581.

[14] F. Fischer, H. Tropsch, *Brennst Chem.* 1923,4,276 – 285.

[15] B. Shi, B. H. Davis, *Catal. Today.* 2005,106,129.

[16] J.N. Chheda, J.A. Dumesic, *Catal. Today*. 2007,123,59.

[17] R.M. West, Z.Y. Liu, M. Peter, C.A. Gartner, J.A. Dumesic, *J. Mol. Catal. A: Chem*. 2008, 296,18.

[18] C.A. Hamilton, S.D. Jackson, G.J. Kelly, *Appl. Catal. A:Gen*. 2004,263,63.

[19] L.G. Wade *Organic Chemistry, (6th ed. 2005), Upper Saddle River, New Jersey: Prentice Hall.*

[20] H. Henschela, M. H. Prosencb, I. A. Nichollsa, *Journal of Molecular Catalysis A:Chemical.* 2011,351,76.

[21] N. Kumagai, S. Matsunaga, N. Yoshikawa, T. Ohshima, M. Shibasaki,*Org. Lett.* 2001, 3,10.

[22] N.Kumagai, S. Matsunaga, T. Kinoshita, S. Harada, S.Okada, S.Sakamoto, K.Yamaguchi, M. Shibasaki, *J. Am. Chem. Soc*. 2003,125,2169.

[23] R. Mahrwald, B. Ziemer, *Tetrahedron Letters*.2002,43,4459.

[24] H. Inoue, M. Kikuchi, J.Ito, H. Nishiyama, *Tetrahedron.* 2008, 64,493-499.

[25] J.I. Di Cosimo,V.K.Diez, C.R.Apesteguia, *Appl.Catal. A*. 1996,137,149.

[26] G. Wang, Z. Zhang, Y.-W. Dong, *Org. Process Res*. *Dev*.2003,8,18.

[27] Y. Shigemasa, K. Yokoyama, H. Sashiwa, H. Saimoto, *Tetrahedron Lett.* 1994, 3,1263.

[28] Z. Zhang, Y.-W. Dong, G.-W. Wang, *Chem. Lett*. 2003,32,966.

[29] C. A. Hamilton, S.D.Jackson, G.J. Kelly. *Applied Catalysis A: General.* 2004,263,63.

[30] Palomares, A. E. Eder-Mirth, G. Rep, M. Lercher, *J. A. J. Catal.*1998,180,56.

[31] R. Zeng, X. Fu, C. Gong, Y. Sui, X. Ma, X. Yang, *J. Mol. Catal. A: Chem*. 2005, 229,1.

[32] B.M. Choudary, M.L. Kantam, P. Sreekanth, T. Bandopadhyay, F. Figueras, A. Tuel, *J. Mol. Catal. A: Chem.* 1999,142,361.

[33] J.C.A.A. Roelofs, D.J. Lensveld, A.J. Dillen, K.P.d. Jong*, J. Catal.* 2001,203,184.

[34] M.J. Climent, A. Corma, S. Iborra, A. Velty, *J. Catal.* 2004,221,474.

[35] M. E.sad, M. Neurock, E. Iglesia, *J.Am.Chem.Soc*. 2011,133,20384.

[36] C. Gardner Swain, Arnet L. Powell, William A. Sheppard, Charles R. Morgan, *J. Am. Chem. Soc.* 1979,101:13, 3576-3583.

[37] H. Berberich, P. W. Roesky, *Angew. Chem. Int. Ed.* 1998,37,11,1569-1571.

[38] T. Akashi, S. Sato, K. Inui, *Catalysis Communication.* 2002,4,411.

[39] G. Kresse, J. Furthmuller, *Comput. Mater. Sci*. 1996, 6,15.

[40] J. Perdew, *Phs.rev.B*.1992, 46,6671.

[41] David Vanderbilt, *Phys. Rev.B.* 1990,41,7892.

[42] G. Mills, H. Jonsson, G.K. Schenter*, Surf. Sci*. 1995,324,305.

[43] H. Jónsson, G. Mills, K.W. Jacobsen, *World Scientific*, Singapore, 1998.

[44] G. Henkelman, B. P. Uberuaga, H. *J.* Jonsson, *J. Chem. Phys.* 2000,113,9901.

[45] G. Henkelman, H. Jonsson, *J. Chem. Phys*. 2000,113,9978

[46] G. Henkelman, H. Jonsson, *J. Chem. Phys.* 1999,111,7010.

[47] A. Heyden, A.T. Bell, F.J. Keil*, J. Chem. Phys*. 2005,123,224101.

[48] X. Qian, J. Li, L. Qi, C.Wang, T.Chan, Y.Yao, K. Ho, S. Yip. *Phys. Rew. B.* 2008,78, 245112.

[49] C. Ammon, A. Bayer, G. Held, B. Richer, T. Schmidt, H.P. Steinrück, *Surf. Sci.* 2002, 507, 845.

[50] P. Hofmann, K.M. Schindler, S. Bao, V. Fritzche, D.E. Ricken, A.M. Bradshaw, D.P. Woodru., *Surf. Sci.* 1994, 304, 74.

[51] M. Witko, K. Hermann, D. Ricken, W. Stenzel, H. Conrad, A.M. Bradshaw, *Chem.Phys.*1993, 177, 363.

[52] A.V. de Carvalho, M.C. Asensio, D.P. Woodru, *Surf. Sci*. 1992, 273, 381.

[53] M.A. Karolewski, R.G. Cavell, *Surf. Sci*.1995, 344, 74.

[54] T.H. Ellis, H. Wang, *Langmuir*. 1994, 10, 4083.

[55] J.P. Camplin, E.M. McCash, *Surf. Sci*. 1996, 360, 229.

[56] C. Ammon, A. Bayer, G. Held, B. Richter, T.Schmidt, H.P. Steinruck, *Surf. Sci.* 2002,845,507-510.

[57] M. Bowker, R. J. Madix, *Surf. Sci.* 1982,116,549.

[58] S. K. Desai, M. Neurock, K. Kourtakis, *J. Phys. Chem. B.* 2002, *106,* 2559-2568.

[59] Y. Ishikawa, M.Liao, R. Carlos, *Cabrera Surface Science.*2000*,*463, 66– 80.

[60] E.D. Batyrev, J.C. van den Heuvel, J. Beckers, W.P.A. Jansen, H.L. Castricum*, J.Catal.* 2005,229,136-143 .

[61] Jensen, William B. The Lewis acid-base concepts: An overview 1979 Wiley

[62] B. N. Zope, D. D. Hibbitts, M. Neurock, R. J. Davis, *Science*. 2010,330 74.

[63] Q.Xing, W. Pei, et al. Fundamental Organic Chemistry. Higher Education Press. China, 2005.

[64] T. Akashi, S. Sato, K. Inui, *Catalysis Communication.* 2002, 4, 411.

[65] D.J. Elliot, F., J. Pennella. *J.Catal*,1989, 119, 359.

[66] Iglesia, Not published.

[67] K Takeshita, S Nakamura, K. Kawamoto, *Bull. Chem.Soc.Jpn*. 1978,51,2622.

[68] R. Mahrwald, B. Ziemer, *Tetrahedron Letters.* 2002,43,4459.

[69] B. Xu, X. Liu, J. Haubrich, R. J. Madix, C. M. Friend, *Angew. Chem. Int. Ed.* 2009,48,4206.

[70] X.Liu, B. Xu, J.Haubrich, R.J. Madix, C. M. Friend, *J. Am.Chem. Soc*. 2009,131,5757.

Appendix

A1 Adsorption Configurations of Propanal, Propanol and their C-H activated species

To facility the illustration, we make a definition that in propanal, the carbon of carbonyl group is C_{car}, the carbon at the α position is C_α and the carbon at the ending position is C_{end}. For propanol, we have the similar definition.

Bare Cu(111) surface is shown in FigA1 (a). In propanal molecule, carbonyl group is the primary functional group and studying its interaction with the metal surface is the primary interest. C=O bond is suggested to adsorb on metal surface either by di-sigma (FigA1 (b), in which C atom and O atom in carbonyl group adsorb on adjacent metal atoms), O-top (FigA1(c), in which only O atom in carbonyl group adsorbs on A-top site of metal) or pi (FigA1 (d), in which C atom and O atom in carbonyl group adsorb on the same metal atom). The adsorption energy of O-top configuration is 18 kJ/mol. For propanol molecule, O-top is the only stable adsorption configuration and it has the adsorption energy of 35 kJ/mol.

The product of C-H activation of propanal makes C_{car}, C_α or C_{end} become unsaturated. There are some different adsorption configurations: C-top (FigA1 (e)), di-sigma, pi, C-top &O-top (Fig.A1 (f)) and sigma-3 (Fig.A1(g)). Generally, the C=O group and the unsaturated carbon would have the possibility to adsorb on metal surface separately or together.

The underscored number in Table A1.1 is the energy for most strongly adsorbed configuration. We can tell that for the product of C_{car} –H activation (CH_3CH_2CO), di-sigma is the most favorable one. For the product of C_α-H ($CH_3C*HCHO$) and C_{end} –H activation ($C*H_2CH_2CHO$), the O-top &C-top configuration is the most stable one.

Different from the C-H activation of propanal, the product of C-H activation of propanol only has two possible positions to adsorb on metal surface: the unsaturated carbon and the oxygen in hydroxyl group. These two adsorption groups could adsorb together or separately. From Table A1.2, we know that for C-H activated species at C_{car} position, both the C-top and C-top & O-top are favored adsorption configurations. For C-H activated species at C_α and C_{end}, the C-top & O-top configurations are the more stable adsorption configuration.
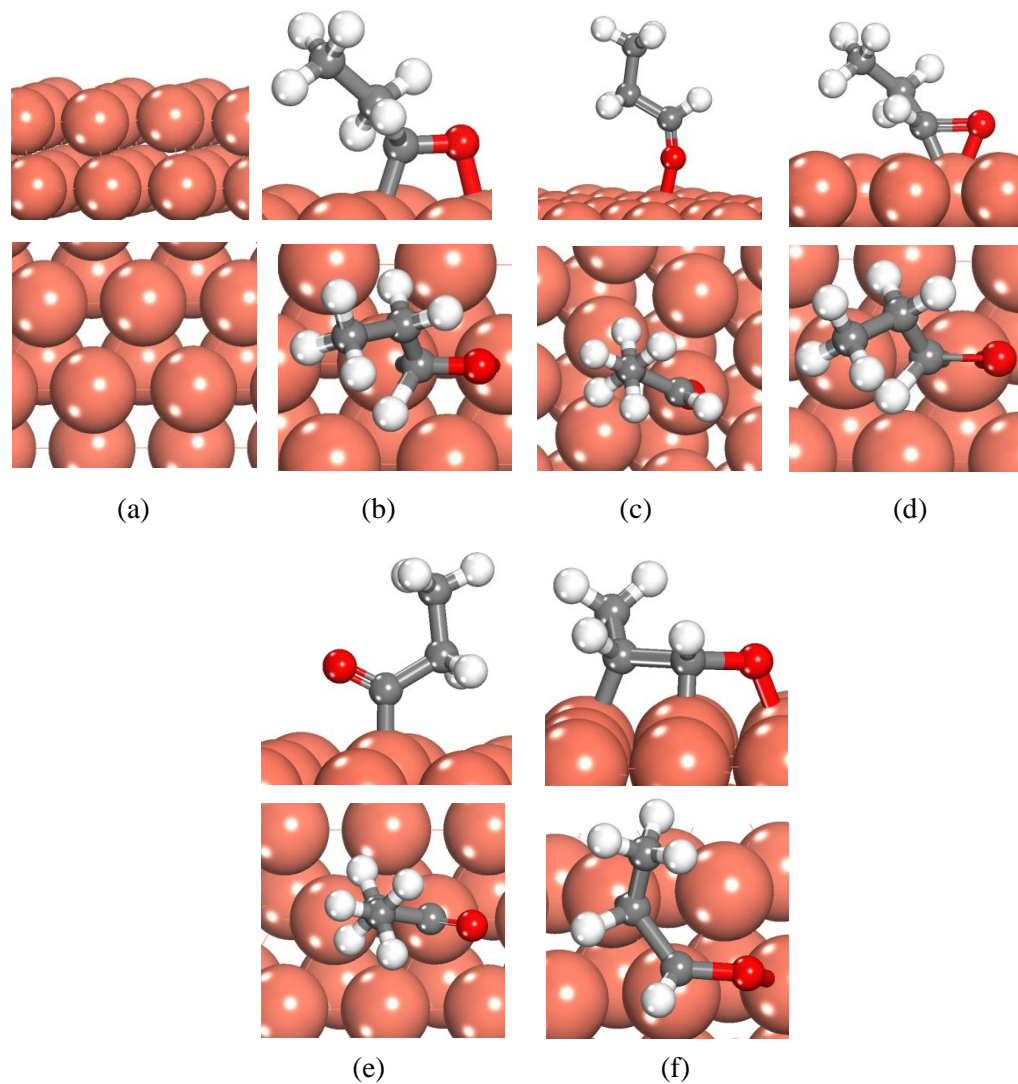
(a)　　　　　(b)　　　　　(c)　　　　　(d)

(e)　　　　　(f)

Fig A1.1 Side (upper panels) and top (bottom panels) view of different adsorption configurations of propanal or C-H activated species. (a) Pure Cu surface; (b) – (d) illustrate the di-sigma, O-top and pi configurations, by using propanal as example; (e) illustrate C-top configuration by using CH_3CH_2C*O as example; (f) illustrate sigma-3 configuration by using $CH_3C*HC*HO*$ as example.

Table A1.1 Adsorption energies (kJ/mol) of different configurations of Propanal C-H Activated species [a]

	Di-sigma	pi	O-top	C-top	O-top & C-top	Sigma3
Propanal	/	/	18	/	/	/
C1-Activated Propanal	**_-159_** [b][c] C-O	-150 [d] C-top	/	-152	/	/
C2-Activated Propanal	/	/	-111 O-top	**_-144_** [e] O-top & C-top	-135	-127
C3-Activated Propanal	/	/	/	-144	**_-161_**	-160 [f] C-O

(a) definition of adsorption configurations are defined in Appendix, part A1 (b) The configuration changes to C-O after optimization (c) numbers with underscore are the most stable adsorption configuration (d) The configuration changes to C-top after optimization (e) The configuration changes to O-top & C-top after optimization (f) The configuration changes to O-top & C-top after optimization

Table A1.2 Adsorption energies (kJ/mol) of different configurations of Propanol C-H activated species

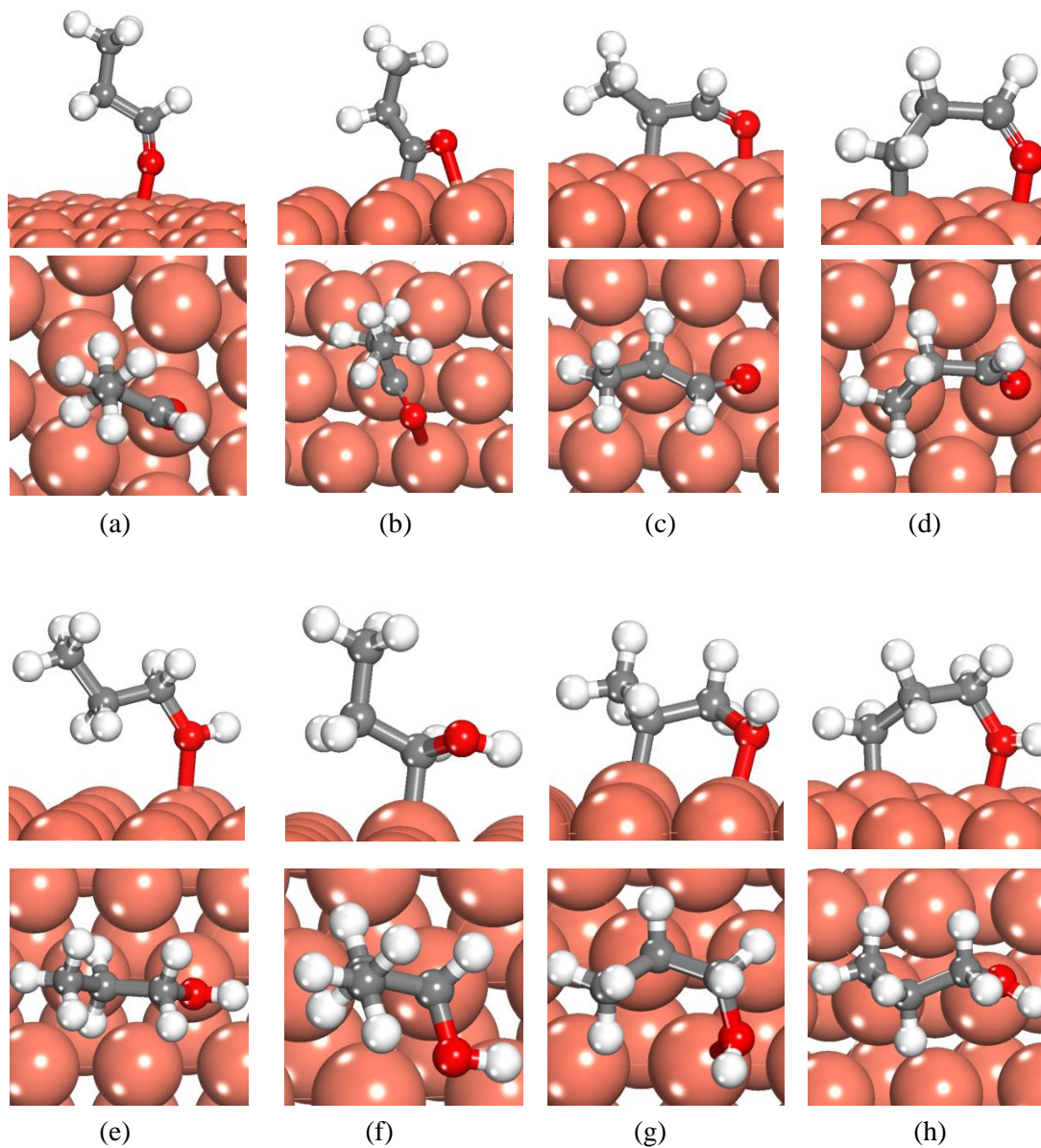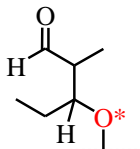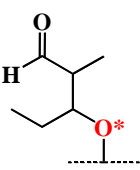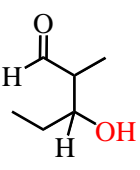|	C-top	O-top & C-top	O-top
Propanol	/	/	35
C1-Activated Propanol	**_-120_**	-118	/
C2-Activated Propanol	**_-150_** **(O&C)**	-142	/
C3-Activated Propanol	-152	**_-159_**	/

Fig A1.2 Side (upper panels) and top (bottom panels) of the most stable adsorption configurations for (a) propanal (b) C_{car} activated product of propanal (c) C_α activated product of propanal (d) C_{end} activated product of propanal (e) propanol (f) C_{car} activated product of propanol (g) C_α activated product of propanol (h) C_{end} activated product of propanol

A2 Adsorption Configurations and Energies of relevant molecules to Aldol Condensation

Only the molecules and derived fragments for the first two steps of aldol condensation are calculated (i.e, coupling + dehydrogenation or coupling + hydrogenation). The different adsorption configurations and energies of relevant molecules are listed in Fig A2.1 and Table A2.1. Generally, there are five different ways of adsorptions: (1) O in carbonyl group (O_c), (2) O in the C-O-C structure (O_{c-o}), (3) both oxygen in carbonyl group and in the C-O-C structure (O_{di}), (4) the carbonyl group C=O and (5) the carbonyl group C=O with the oxygen in C-O-C group (C=O& O_{c-o}). For the product of coupling between enolate and propanal (Table A2.1(a), Fig A2.1(a)), the most stable configuration is O_{c-o} with adsorption energy of 208 kJ/mol. For the dehydrogenated structure of this coupling product (Table A2.1(b), Fig A2.1(b)), O_{di} adsorption configuration is the favored structure. For the hydrogenated molecule of the coupling product (Table A2.1(c), Fig A2.1(c)), O_{c-o} has an adsorption energy of 28 kJ/mol and this is the preferred adsorption configuration.

Table A2.1 Adsorption energies (kJ/mol) of adsorption configurations of relevant molecules for Aldol Condensation

Molecule	Adsorption Position	Adsorption Energy (kJ/mol)
(a)	O_{c-o}	*-208*
	O_{di}	-192
	C=O & O c-o	-204 (move to O c-o)
(b)	O_c	-24
	O_{c-o}	-24(move to di)
	O_{di}	*-28*
	C=O and O in C-O-C	-17 (Move to O c-o)
	C=O	*-28 (Move to O c-o)*
(c)	O_c	-19
	O_{c-o}	*-35*
	O_{di}	-14
	C=O and O_{c-o}	-23
	C=O	-5 (move to Oc)

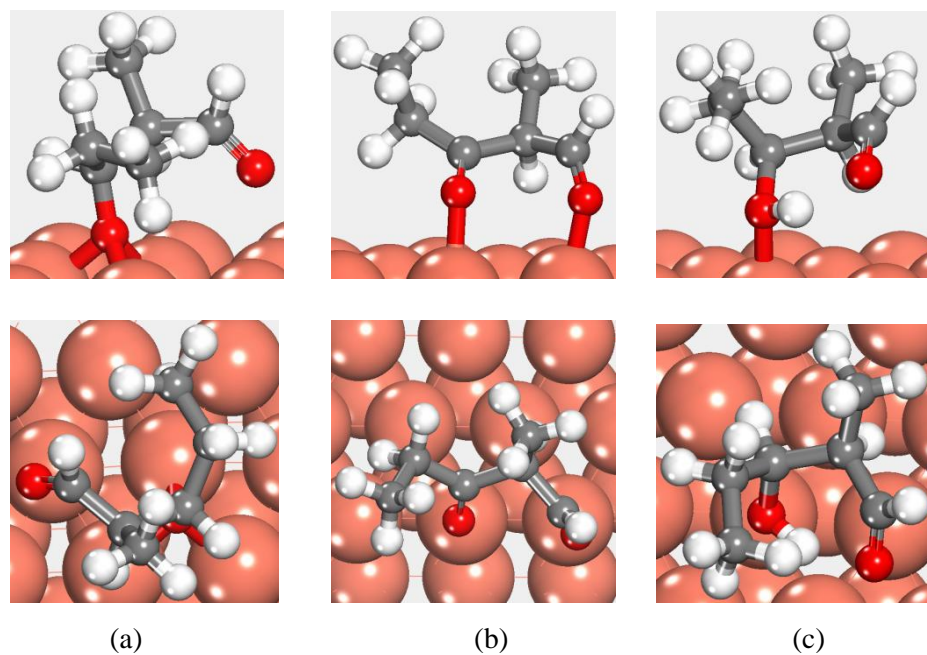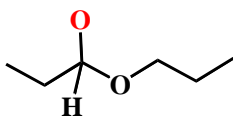(a)   (b)   (c)
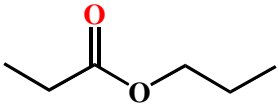
Fig A2.1 Side (upper panels) and top (bottom panels) view of the most stable adsorption configurations for (a) C-C coupling product (b) dehydrogenation product for C-C coupling product and (c) hydrogenation product for C-C coupling product in aldol condensation reaction.

A3 Adsorption Configurations and Energies of relevant molecules of Esterification

Similar with aldol condensation, there are up to five adsorption configurations for relevant molecules and derived fragments involved in esterification. Table A3.1 lists all of them. For either the molecule produced from coupling between alkoxide and propanal or the final ester molecule, the most stable configuration for the product of coupling is O_c, in which the oxygen comes from the previous aldehyde adsorbs on metal surface.

Table A3.1 Adsorption energies (kJ/mol) of adsorption configurations of relevant molecules for Esterification

Molecule	Adsorption Position	Adsorption Energy (kJ/mol)
(a)	O_c	**-214**
	O_{c-o}	-204 (move to $O_{di}^{(a)}$)
	O_{di}	-204
(c)	O_c	-30
	O_{c-o}	-28(move to O_c)
	O_{di}	**-31(move to O_c)**
	C=O	
	C=O with O c-o	**-31(move to O_c)**

(a) It means the initial O_{c-o} structure moves to O_{di} structure after optimization

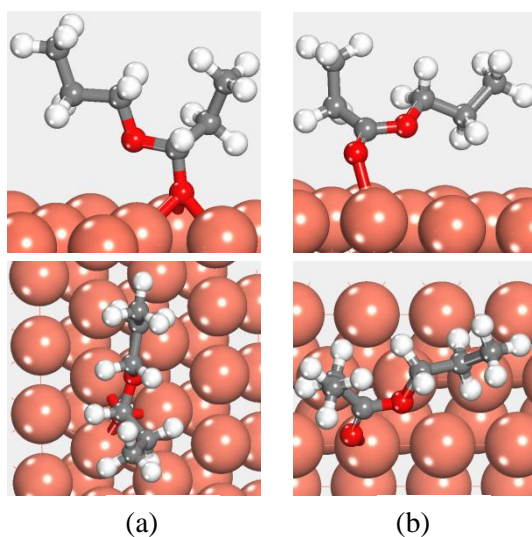(a)   (b)

Fig A3.1 Side (upper panels) and top (bottom panels) view of the most stable adsorption configurations for (a) C-O coupling product between propoxide and paopanal (b) ester, the dehydrogenation product for C-O coupling product